PHYSICAL REVIEW D **96,** 075006 (2017)

Probing Majorana neutrino textures at DUNE

Kalpana Bora,[1,*] Debasish Borah,[2,†] and Debajyoti Dutta[3,4,‡]

[1]*Department of Physics, Gauhati University, Guwahati, Assam 781014, India*
[2]*Department of Physics, Indian Institute of Technology Guwahati, Assam 781039, India*
[3]*Harish-Chandra Research Institute, Chhatnag Road, Jhunsi, Allahabad 211019, India*
[4]*Homi Bhabha National Institute, Training School Complex, Anushaktinagar, Mumbai 400094, India*

(Received 17 November 2016; published 6 October 2017)

We study the possibility of probing different texture zero neutrino mass matrices at the long baseline neutrino experiment DUNE, particularly focusing on its sensitivity to the octant of atmospheric mixing angle θ_{23} and leptonic Dirac CP phase $\delta_{\rm cp}$. Assuming a diagonal charged lepton basis and Majorana nature of light neutrinos, we first classify the possible light neutrino mass matrices with one and two texture zeros and then numerically evaluate the parameter space which satisfies the texture zero conditions. Apart from using the latest global fit 3σ values of neutrino oscillation parameters, we also use the latest bound on the sum of absolute neutrino masses ($\sum_i |m_i|$) from the Planck mission data and the updated bound on effective neutrino mass M_{ee} from neutrinoless double beta decay ($0\nu\beta\beta$) experiments to find the allowed Majorana texture zero mass matrices. For the allowed texture zero mass matrices from all these constraints, we then feed the corresponding light neutrino parameter values satisfying the texture zero conditions into the numerical analysis in order to study the capability of DUNE to allow or exclude them once it starts taking data. We find that DUNE will be able to exclude some of these texture zero mass matrices which restrict (θ_{23}-$\delta_{\rm cp}$) to a very specific range of values, depending on the values of the parameters that nature has chosen.

DOI: 10.1103/PhysRevD.96.075006

I. INTRODUCTION

Since the discovery of the Higgs boson in 2012, the large hadron collider (LHC) experiment has been confirming the validity of the standard model (SM) of particle physics again and again without any convincing signature of new physics beyond the standard model (BSM) to date. In spite of such null results, there are plenty of reasons, both theoretical and observational, which undoubtedly suggest the presence of BSM physics. The observation of tiny but nonzero neutrino masses and large leptonic mixing by neutrino oscillation experiments [1–7] is one such reason that has led to a large number of BSM proposals in the last few decades. The current status of neutrino oscillation experiments can be summarized in terms of the 3σ global fit values of neutrino parameters shown in Table I, where NH and IH refer to normal and inverted hierarchical neutrino masses, respectively.

The data in Table I also allow the possibility of quasidegenerate neutrinos ($m_1 \approx m_2 \approx m_3$). Although the question of the absolute mass scale of neutrinos remains open in oscillation experiments, cosmology and neutrinoless double beta decay ($0\nu\beta\beta$) experiments put an upper bound on the lightest neutrino mass. For example, the latest Planck experiment data constrain the sum of absolute neutrino masses to $\sum_i |m_i| < 0.17$ eV [8]. Similarly, constraints from the ongoing $0\nu\beta\beta$ experiments [9–12] rule out light neutrino masses around 0.1 eV and above. On the other hand, the leptonic Dirac CP phase $\delta_{\rm cp}$ remains undetermined as of now, though a recent hint towards $\delta_{\rm cp} \approx -\pi/2$ [13] appeared recently from the T2K Collaboration. If neutrinos are Majorana fermions, then two Majorana CP phases come into the picture—which, however, do not affect neutrino oscillation probabilities, but can be probed in $0\nu\beta\beta$ experiments.

In the three-flavor neutrino oscillation scenario, the oscillations are driven by the two mass-square differences Δm^2_{21} and $|\Delta m^2_{31}|$. Out of the three mixing angles θ_{12}, θ_{13}, and θ_{23} governing the oscillation amplitudes, θ_{12} and θ_{13} are very precisely measured. Although the atmospheric mixing angle θ_{23} was measured in 1998 in the Super-Kamiokande

TABLE I. Global fit 3σ values of neutrino oscillation parameters [14]. Here $\Delta m^2_{3l} \equiv \Delta m^2_{31}$ for NH, and $\Delta m^2_{3l} \equiv \Delta m^2_{32}$ for IH.

Parameters	Normal hierarchy (NH)	Inverted hierarchy (IH)
$\frac{\Delta m^2_{21}}{10^{-5}\ \text{eV}^2}$	7.03–8.09	7.02–8.09
$\frac{\lvert\Delta m^2_{3l}\rvert}{10^{-3}\ \text{eV}^2}$	2.407–2.643	2.399–2.635
$\sin^2\theta_{12}$	0.271–0.345	0.271–0.345
$\sin^2\theta_{23}$	0.385–0.635	0.393–0.640
$\sin^2\theta_{13}$	0.01934–0.02392	0.01953–0.02408
δ	0°–360°	145°–390°

*kalpana.bora@gmail.com
†dborah@iitg.ernet.in
‡debajyotidutta@hri.res.in

 © 2017 American Physical Society

atmospheric neutrino experiment, it is not yet confirmed if $\theta_{23} = 45°$—i.e. if it is maximal or not. If not, then it may lie either in the higher octant (HO) ($\theta_{23} > 45°$) or in the lower octant (LO) ($\theta_{23} < 45°$). The preliminary results from the T2K experiment [3,13] prefer near maximal mixing [15], while MINOS [7,16] and Super-Kamiokande (SK) disfavor maximal mixing [17]. All the global fit analyses are inconsistent with maximal θ_{23} at less than 1σ [14,18]. Recent NOνA data exclude the maximal mixing scenario at a 2.5σ C.L. [19], favoring the case of two degenerate solutions. So in the present scenario, we have to wait for the long baseline (LBL) accelerator experiments to resolve this ambiguity, as well as to measure θ_{23} precisely. The capability of DUNE (Deep Underground Neutrino Experiment) [20–23], NOνA [24,25], T2K, etc. to resolve octant ambiguity has been studied in Refs. [26–28]. Octant sensitivity at DUNE in conjunction with reactor experiments is studied in Refs. [29,30]. These long baseline accelerator experiments are sensitive to both $\nu_\mu \to \nu_e$ (appearance) and $\nu_\mu \to \nu_\mu$ (disappearance), and synergy between them can enhance the octant sensitivity [31–33]. On the other hand, any terrestrial baseline of several hundred kilometers is sensitive to matter effects. So these LBL experiments, being sensitive to matter effects, can discriminate between the two hierarchies [20,34].

After the precise measurement of θ_{13}, now the whole neutrino community is focusing on the leptonic Dirac CP phase $\delta_{\rm cp}$, which is the only unknown parameter in the three-flavor oscillation framework. Although in the quark sector, CP violation is observed and can be explained due to complex Yukawa couplings or complex Higgs field vacuum expectation values [35,36], it is yet to be discovered in the leptonic sector with some significant degree of precision. The LBL accelerator experiments which are sensitive to the $\nu_\mu \to \nu_e$ channel can probe CP violation in the leptonic sector [20]. From this point of view, DUNE at Fermilab in the U.S. is the best candidate, which will start taking data in the next decade. In the literature, recent studies related to the CP violation discovery potential of DUNE as well as other superbeam experiments can be found [37–41].

Before the neutrino oscillation experiments completely remove the existing ambiguities in neutrino parameters like the octant of θ_{23} and the Dirac CP phase, as well as the mass hierarchy at ongoing and near future facilities, it is important to study the predictions for these neutrino observables within different BSM frameworks. Depending on the predictions for such neutrino observables, one can discriminate between different BSM scenarios in the oscillation experiments. However, generic BSM frameworks come with several free parameters, making it difficult to have a robust prediction for a particular neutrino parameter. Reducing the number of free parameters can therefore lead to robust, testable predictions of neutrino observables. Such reduction of free parameters can be possible within the framework of flavor symmetry models where the additional discrete or continuous symmetries either relate two or more terms or forbid some terms in the mass matrix. One such possibility arises within the context of texture zeros in leptonic mass matrices. For a complete survey of such texture zeros in lepton mass matrices, please refer to Ref. [42]. Different possible flavor symmetric interpretations for the origin of such texture zero mass matrices can be found in Refs. [43–52] within the framework of different seesaw models. Such texture zero mass matrices, in general, have specific predictions for neutrino oscillation parameters, the consequences of which can be studied from cosmology as well as from an oscillation experiment's point of view. In the light of neutrino oscillation experiment data, one-zero and two-zero texture mass matrices were studied in Refs. [53–56] and [52,57–69], respectively. These texture zero mass matrices were also studied from the perspective of baryogenesis through leptogenesis in Refs. [70–76].

In this work, we do a phenomenological study of one-zero and two-zero texture mass matrices, assuming the neutrinos to be of Majorana nature and the charged lepton mass matrix to be diagonal. The main motive of this work is twofold. First, we intend to find out the allowed texture zero mass matrices from the requirement of satisfying the latest neutrino oscillation data as well as the cosmological bound on the sum of absolute neutrino masses from the latest Planck mission data [8] and the bound on effective neutrino mass M_{ee} from the latest experimental lower bound on neutrinoless double beta decay half-life [11,12]. The second objective is to find if any of these textures which are allowed from all experimental constraints can be probed, focusing on the sensitivity of neutrino oscillation experiments like DUNE to the values of θ_{23}, $\delta_{\rm cp}$ predicted by a particular texture zero mass matrix. We first numerically determine the values of θ_{23}, $\delta_{\rm cp}$ along with other neutrino parameters which satisfy a particular texture zero condition and then use them in GLoBES software [77,78] to determine the corresponding experimental sensitivity. We show that these textures can be excluded for some combinations of θ_{23} and $\delta_{\rm cp}$ at DUNE. If nature chooses some values of θ_{23} and $\delta_{\rm cp}$, then determining how DUNE can allow or exclude a particular mass matrix texture is the goal of this present study. We have found that the two-zero textures are very interesting, as DUNE can constrain the θ_{23}-$\delta_{\rm cp}$ parameter space more tightly compared to the one-zero textures. We have observed that if nature prefers normal (inverted) mass ordering, then DUNE can constrain a particular type of texture mass matrix denoted as B1 (B1 and B2) more tightly than any other textures.

This article is organized as follows: In Sec. II, we discuss the different possible texture zero mass matrices. A brief discussion on DUNE is presented in Sec. III. Section IV contains the details of our numerical analysis, while in

Sec. V we present our results and discussions. Concluding remarks are given in Sec. VI.

II. TEXTURE ZEROS IN A MAJORANA NEUTRINO MASS MATRIX

If light neutrinos are of Majorana nature, the 3×3 mass matrix M_ν is complex symmetric, having six independent complex parameters. In such a scenario, the total number of structurally different Majorana neutrino mass matrices with k texture zeros is given by

$$ {}^6C_k = \frac{6!}{k!(6-k)!}. \tag{1}$$

A symmetric mass matrix with more than three texture zeros is not compatible with the observed leptonic mixing and masses. The Pontecorvo-Maki-Nakagawa-Sakata (PMNS) leptonic mixing matrix is related to the diagonalizing matrices of charged lepton and neutrino mass matrices as

$$ U_{\rm PMNS} = U_l^\dagger U_\nu. \tag{2}$$

In the diagonal charged lepton basis, $U_{\rm PMNS}$ is the same as the diagonalizing matrix U_ν of the neutrino mass matrix M_ν. In this basis, it was shown [79] that a symmetric Majorana neutrino mass matrix with three texture zeros is not compatible with neutrino oscillation data. This leaves us with the possible one-zero and two-zero texture mass matrices. Going by the counting formula mentioned above (1), we can have six possible one-zero texture and 15 possible two-zero texture mass matrices. The one-zero texture mass matrices can be written as

$$ G_1: \begin{pmatrix} 0 & \times & \times \\ \times & \times & \times \\ \times & \times & \times \end{pmatrix}, \quad G_2: \begin{pmatrix} \times & 0 & \times \\ 0 & \times & \times \\ \times & \times & \times \end{pmatrix}, $$
$$ G_3: \begin{pmatrix} \times & \times & 0 \\ \times & \times & \times \\ 0 & \times & \times \end{pmatrix}, \quad G_4: \begin{pmatrix} \times & \times & \times \\ \times & 0 & \times \\ \times & \times & \times \end{pmatrix}, $$
$$ G_5: \begin{pmatrix} \times & \times & \times \\ \times & \times & 0 \\ \times & 0 & \times \end{pmatrix}, \quad G_6: \begin{pmatrix} \times & \times & \times \\ \times & \times & \times \\ \times & \times & 0 \end{pmatrix}, \tag{3}$$

where the crosses "×" denote nonzero arbitrary elements of M_ν. Similarly, the two-zero texture matrices, classified into six categories (following the notations of Ref. [65]), are given by

$$ A_1: \begin{pmatrix} 0 & 0 & \times \\ 0 & \times & \times \\ \times & \times & \times \end{pmatrix}, \quad A_2: \begin{pmatrix} 0 & \times & 0 \\ \times & \times & \times \\ 0 & \times & \times \end{pmatrix}; \tag{4}$$

$$ B_1: \begin{pmatrix} \times & \times & 0 \\ \times & 0 & \times \\ 0 & \times & \times \end{pmatrix}, \quad B_2: \begin{pmatrix} \times & 0 & \times \\ 0 & \times & \times \\ \times & \times & 0 \end{pmatrix}, $$
$$ B_3: \begin{pmatrix} \times & 0 & \times \\ 0 & 0 & \times \\ \times & \times & \times \end{pmatrix}, \quad B_4: \begin{pmatrix} \times & \times & 0 \\ \times & \times & \times \\ 0 & \times & 0 \end{pmatrix}; \tag{5}$$

$$ C: \begin{pmatrix} \times & \times & \times \\ \times & 0 & \times \\ \times & \times & 0 \end{pmatrix}; \tag{6}$$

$$ D_1: \begin{pmatrix} \times & \times & \times \\ \times & 0 & 0 \\ \times & 0 & \times \end{pmatrix}, \quad D_2: \begin{pmatrix} \times & \times & \times \\ \times & \times & 0 \\ \times & 0 & 0 \end{pmatrix}; \tag{7}$$

$$ E_1: \begin{pmatrix} 0 & \times & \times \\ \times & 0 & \times \\ \times & \times & \times \end{pmatrix}, \quad E_2: \begin{pmatrix} 0 & \times & \times \\ \times & \times & \times \\ \times & \times & 0 \end{pmatrix}, $$
$$ E_3: \begin{pmatrix} 0 & \times & \times \\ \times & \times & 0 \\ \times & 0 & \times \end{pmatrix}; \tag{8}$$

$$ F_1: \begin{pmatrix} \times & 0 & 0 \\ 0 & \times & \times \\ 0 & \times & \times \end{pmatrix}, \quad F_2: \begin{pmatrix} \times & 0 & \times \\ 0 & \times & 0 \\ \times & 0 & \times \end{pmatrix}, $$
$$ F_3: \begin{pmatrix} \times & \times & 0 \\ \times & \times & 0 \\ 0 & 0 & \times \end{pmatrix}; \tag{9}$$

where the crosses "×" imply nonzero arbitrary elements of M_ν. The latest neutrino oscillation data on mixing angles, mass-squared differences, and cosmology data on the sum of absolute neutrino masses allow only six different two-zero textures $A_{1,2}$ and $B_{1,2,3,4}$, as shown by Refs. [65,67].

III. DUNE AT A GLANCE

The Deep Underground Neutrino Experiment (DUNE) is a future accelerator-based experiment capable of answering

TABLE II. Systematic uncertainties for DUNE.

Experiment	Signal	Signal norm error	Background norm error	Calibration error: Signal	Calibration error: Background
DUNE	ν_e	2%	10%	5%	5%
	ν_μ	5%	10%	5%	5%

all of the three major issues in the neutrino sector mentioned earlier: (a) determination of neutrino mass hierarchy, (b) resolution of the octant of θ_{23}, and (c) determination of leptonic CP violation. The first test with the megawatt neutrino-beam facility will begin in ~2026, and the experiment itself will be fully operational in ~2027 [80,81]. DUNE is designed in such a way that it can answer all three of the most important questions in the neutrino sector mentioned above. The $\nu_\mu(\bar{\nu}_\mu)$ superbeam from the Fermilab will be detected by a 35–40 kton liquid argon (LAr) far detector at a distance of 1300 km in the Homestake mine, South Dakota. The experiment is planned to run for 10 years, both in antineutrino (5 years) and neutrino (5 years) modes. A 1.2 MW, 120 GeV proton beam will deliver 10^{21} protons on target (POT) per year, which corresponds to a total exposure of 35×10^{22} kton-POT-yr.

All other details such as signal and background uncertainties, efficiencies are taken from Refs. [22,23] and are tabulated in Tables II and III.

IV. NUMERICAL ANALYSIS

In the diagonal charged lepton basis, $U_{\rm PMNS}$ is the same as the diagonalizing matrix U_ν, which can be parametrized as

$$U_{\rm PMNS} = \begin{pmatrix} c_{12}c_{13} & s_{12}c_{13} & s_{13}e^{-i\delta_{\rm cp}} \\ -s_{12}c_{23} - c_{12}s_{23}s_{13}e^{i\delta_{\rm cp}} & c_{12}c_{23} - s_{12}s_{23}s_{13}e^{i\delta_{\rm cp}} & s_{23}c_{13} \\ s_{12}s_{23} - c_{12}c_{23}s_{13}e^{i\delta_{\rm cp}} & -c_{12}s_{23} - s_{12}c_{23}s_{13}e^{i\delta_{\rm cp}} & c_{23}c_{13} \end{pmatrix} \mathrm{diag}(1, e^{i\alpha}, e^{i(\beta+\delta_{\rm cp})}), \tag{10}$$

where $c_{ij} = \cos\theta_{ij}$, $s_{ij} = \sin\theta_{ij}$. $\delta_{\rm cp}$ is the Dirac CP phase, and α, β are the Majorana CP phases. Using the parametric form of the PMNS matrix shown in Eq. (10), the Majorana neutrino mass matrix M_ν can be found as

$$M_\nu = U_{\rm PMNS} M_\nu^{\rm diag} U_{\rm PMNS}^T, \tag{11}$$

where

$$M_\nu^{\rm diag} = \begin{pmatrix} m_1 & 0 & 0 \\ 0 & m_2 & 0 \\ 0 & 0 & m_3 \end{pmatrix}, \tag{12}$$

with m_1, m_2, and m_3 being the three neutrino mass eigenvalues. For the case of normal hierarchy, the three neutrino mass eigenvalues can be written as

$$M_\nu^{\rm diag} = \mathrm{diag}\left(m_1, \sqrt{m_1^2 + \Delta m_{21}^2}, \sqrt{m_1^2 + \Delta m_{31}^2}\right),$$

while for the case of inverted hierarchy, they can be written as

$$M_\nu^{\rm diag} = \mathrm{diag}\left(\sqrt{m_3^2 + \Delta m_{23}^2 - \Delta m_{21}^2}, \sqrt{m_3^2 + \Delta m_{23}^2}, m_3\right).$$

The analytical expressions of the elements of this mass matrix are given in the Appendix.

From the parametrization of the light neutrino mass matrix, it can be seen that there are nine parameters: three masses, three angles, and three phases. Out of these, five parameters—namely, two mass-squared differences and three mixing angles—are measured in several experiments, and their best-fit values along with 3σ ranges are shown in Table I. It is worth noting that there still remains some ambiguity in determining the octant of θ_{23}. Apart from this, the three CP phases and the lightest neutrino mass, and

TABLE III. Simulation details like signal efficiencies, energy resolutions, total exposures, and detector mass for DUNE.

Experiment	Signal	Signal Efficiencies	Energy Resolutions	Runtime (yrs) $\nu + \bar{\nu}$	Detector Mass (Type)
DUNE	ν_e^{CC}	80%	$0.15/\sqrt{E}$	$5 + 5$	35 kton (LArTPC)
	ν_μ^{CC}	85%	$0.20/\sqrt{E}$		

hence the type of mass hierarchy, are yet to be determined experimentally. Due to the predictive nature of texture zero mass matrices and upcoming neutrino experiments like DUNE having the potential to settle the issues of the θ_{23} octant and the Dirac CP phase $\delta_{\rm cp}$, as well as the mass hierarchy, we first numerically evaluate the neutrino parameters for a particular texture zero mass matrix using the 3σ values of two angles θ_{12}, θ_{13}, two mass-squared differences from the global fit Ref. [14]. For each possible one-zero texture mass matrix, we have one complex or two real equations which can be solved numerically to evaluate θ_{23}, $\delta_{\rm cp}$ along with restricting other parameters. For the one-zero texture mass matrices, we solve the two real equations corresponding to the texture zero condition and determine the parameter space in terms of neutrino parameters. While solving these equations, we vary the lightest neutrino mass in the range 10^{-6}–0.1 eV and the Majorana CP phases in the range $-\pi < \alpha, \beta < \pi$.

To use the bound on neutrino parameters from $0\nu\beta\beta$ experiments, we use the standard light neutrino contribution to this rare decay process. This rare decay is a lepton-number-violating process where a heavier nucleus decays into a lighter one and two electrons $(A, Z) \to (A, Z+2) + 2e^-$ without any (anti)neutrinos in the final state, thereby violating the lepton number by 2 units. For a review on $0\nu\beta\beta$, please refer to Ref. [82]. The amplitude of the light-neutrino contribution to $0\nu\beta\beta$ can be written as

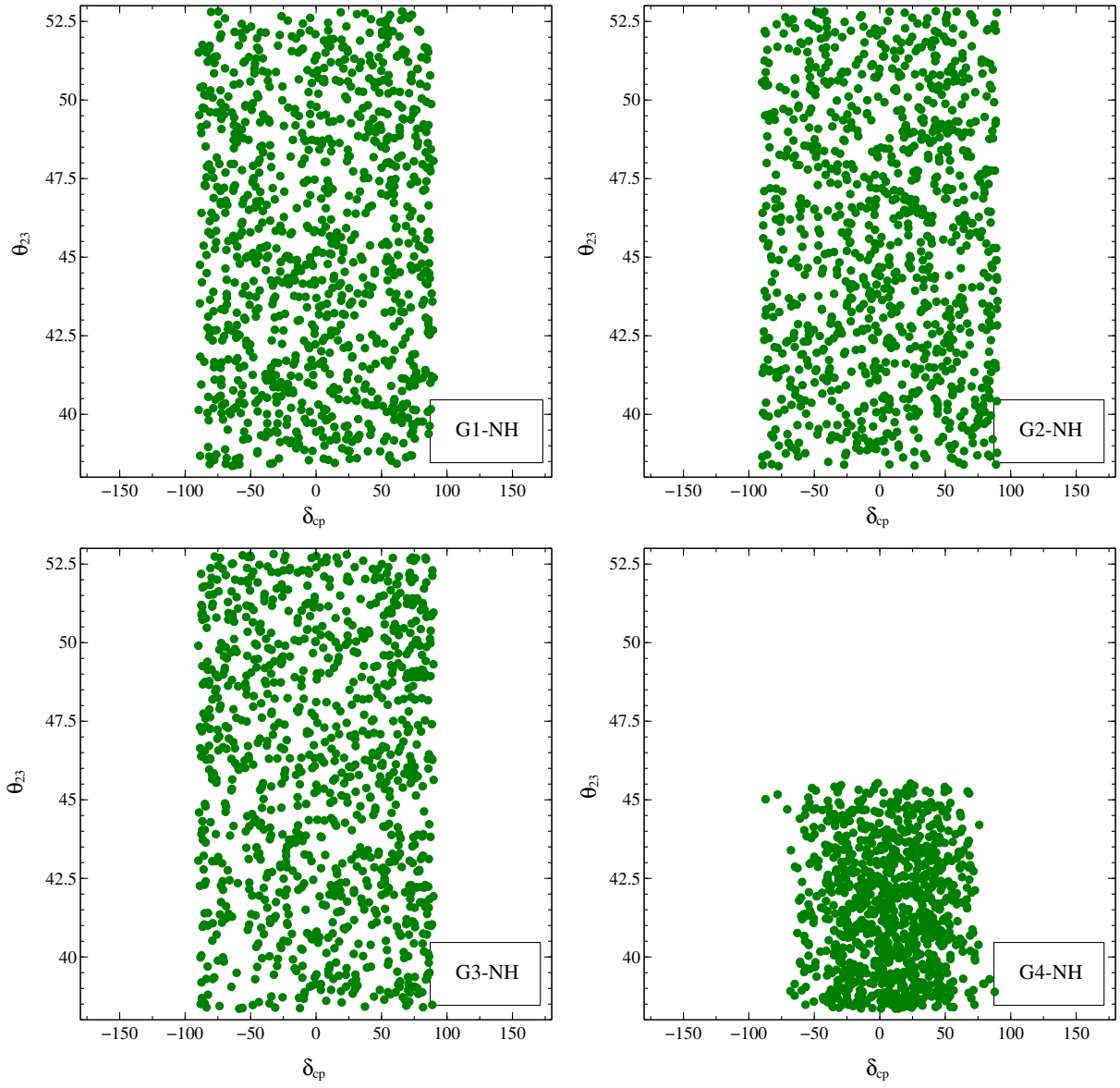

FIG. 1. Neutrino parameters corresponding to one-zero textures for NH.

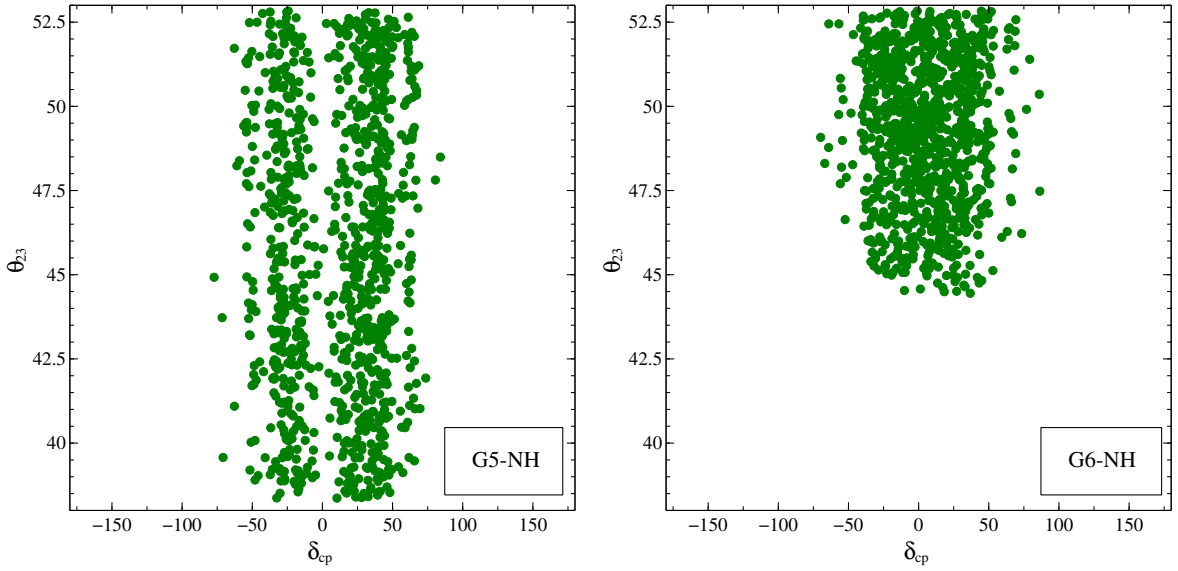

FIG. 2. Neutrino parameters corresponding to one-zero textures for NH.

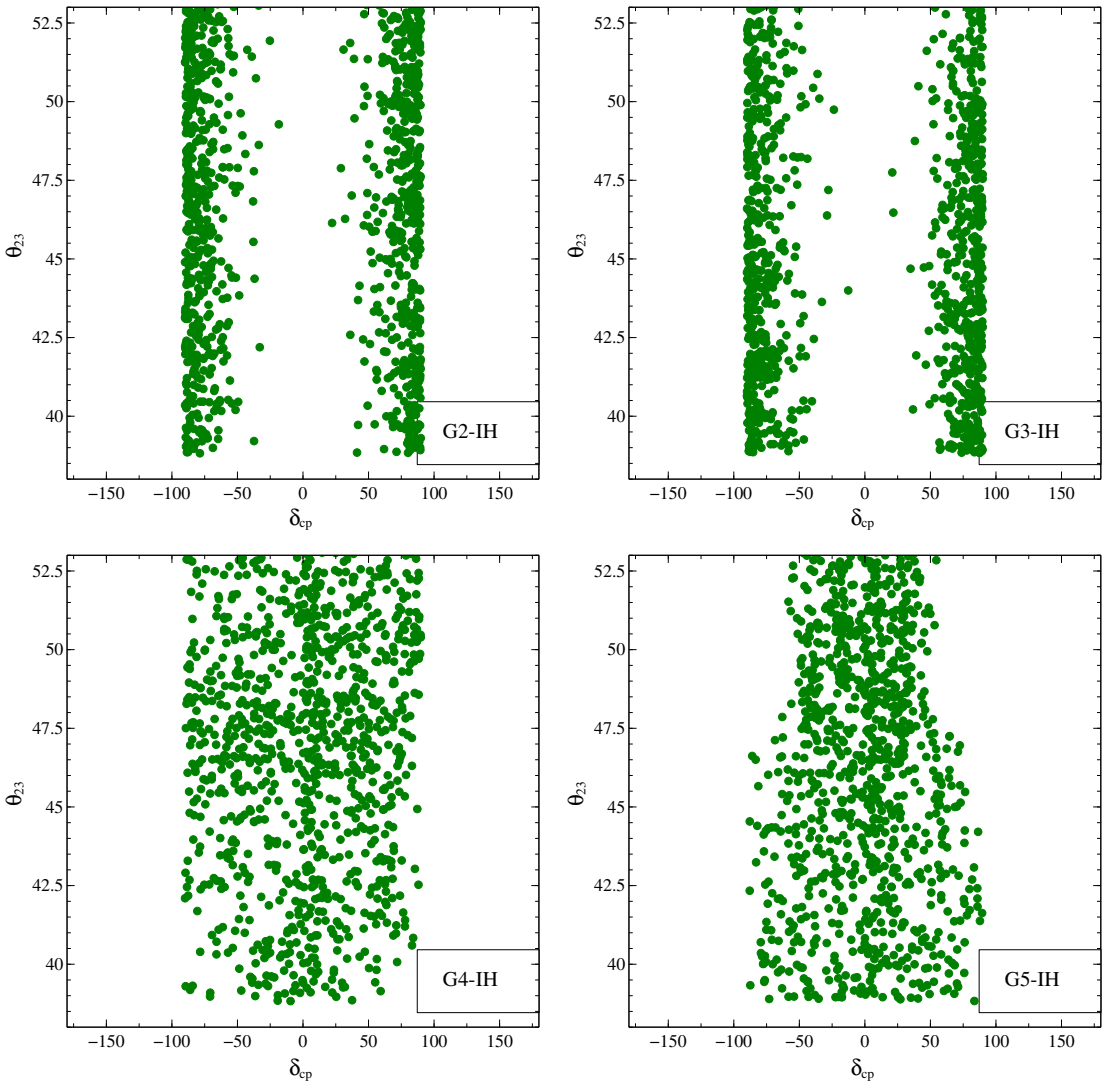

FIG. 3. Neutrino parameters corresponding to one-zero textures for IH.

$$A_{\nu LL} \propto G_F^2 \sum_i \frac{m_i U_{ei}^2}{p^2}, \tag{13}$$

with p being the average momentum exchange for the process. In the above expression, m_i are the masses of light neutrinos for $i = 1, 2, 3$. $G_F = 1.17 \times 10^{-5}$ GeV^{-2} is the Fermi coupling constant, and $U = U_{\rm PMNS}$ is the light neutrino mixing matrix. The corresponding half-life can be written as

$$\frac{1}{T_{1/2}^{0\nu}} = G_{01}^{0\nu} |\mathcal{M}_\nu^{0\nu}(\eta_\nu^L)|^2, \tag{14}$$

where $\eta_\nu^L = \sum_i \frac{m_i U_{ei}^2}{m_e} = \frac{M_{ee}}{m_e}$. Here m_e is the mass of the electron, $\mathcal{M}_\nu^{0\nu}$ is the nuclear matrix element (NME), and $G_{01}^{0\nu}$ is the phase-space factor. Since the ongoing experiments have not observed this rare decay process, they give a lower bound on its half-life, or equivalently, an upper bound on the amplitude. The latest data from the KamLAND-Zen experiment in 2016 have given a lower limit on the $0\nu\beta\beta$ half-life of $T_{1/2}^{0\nu} > 1.07 \times 10^{26}$ yr at a 90% confidence level [11]. Using the commonly adopted values of NME, this lower bound on the half-life corresponds to an upper bound on the effective Majorana neutrino mass in the range $|M_{ee}| < 0.061$–0.165 eV. More recently in 2017, the GERDA Collaboration has given a similar but slightly weaker lower bound on the half-life as $T_{1/2}^{0\nu} > 5.3 \times 10^{25}$ yr at a 90% confidence level [12], which corresponds to an upper bound $|M_{ee}| < 0.15$–0.33 eV.

We use the most conservative bound from the KamLAND-Zen collaboration to constrain the texture zero mass matrices in our analysis. Along with this, we also use the cosmology bound on the sum of absolute neutrino masses $\sum_i |m_i| < 0.17$ eV from the Planck Collaboration results [8] that appeared in 2015.

After numerically evaluating the neutrino oscillation parameters for the texture zero mass matrices, we move on to studying the capabilities of DUNE to exclude these textures once it starts taking data. For this, we have used the present best-fit values of the standard 3ν oscillation parameters as the "true values" or "data." The best-fit values of the oscillation parameters are taken from Ref. [14]. To test a particular texture, the values of the neutrino oscillation parameters from the texture zero conditions are used as "fit" values, and then χ^2 is calculated between "data" and "fit." We define χ^2 (statistical) as

$$\chi^2 = \sum_i \sum_{j=1}^{2} \frac{[N_{i,j}^{\rm true} - N_{i,j}^{\rm test}]^2}{N_{i,j}^{\rm true}}, \tag{15}$$

where $N_{i,j}^{\rm true}$ and $N_{i,j}^{\rm test}$ are the event rates that correspond to "data" and "fit." Here, index i corresponds to the number of bins, and j corresponds to the type of neutrinos, i.e. $j = 1$ for neutrinos and $j = 2$ for antineutrinos. We have considered 39 bins for DUNE in the energy range 0.5–10 GeV having a bin width of 250 MeV. The systematic uncertainties like signal- and background-related uncertainties and calibration errors are introduced in χ^2 by the pull

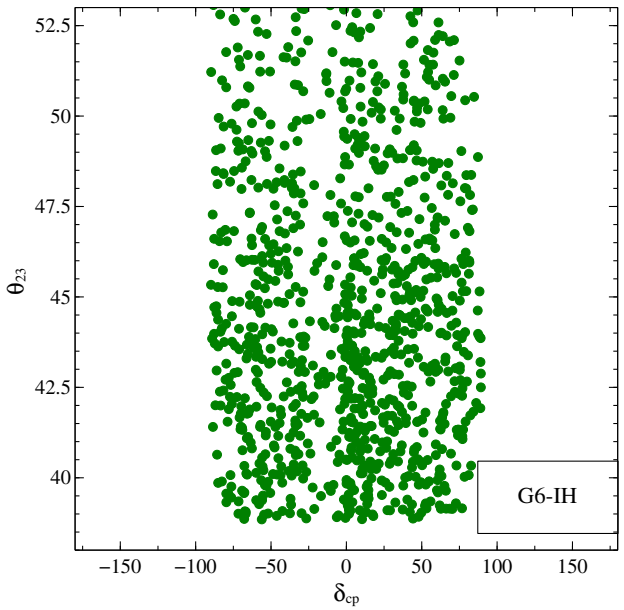

FIG. 4. Neutrino parameters corresponding to the one-zero texture G_6 for IH.

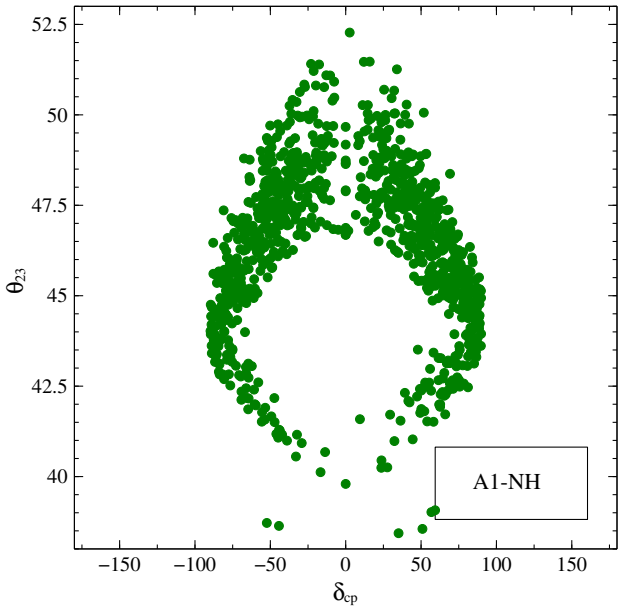

FIG. 5. Neutrino parameters corresponding to the two-zero texture A_1 for NH.

method, and they are allowed to deviate from their standard values in the calculation of the expected rate in the $\{i,j\}$th bins $N_{i,j}^{test}$. If the kth input gets deviated from its standard value by $\sigma_k\xi_k$, then our final modified χ^2 will be

$$\chi^2(\xi_k)=\sum_i\sum_{j=1}^{2}\frac{[N_{i,j}^{test}(std)+\sum_{k=1}^{\text{npull}}c_{i,j}^{k}\xi_k-N_{i,j}^{true}]}{N_{i,j}^{true}}+\sum_{k=1}^{\text{npull}}\xi_k^2,$$

and hence,

$$\chi^2_{\text{pull}}=\min_{\xi_k}[\chi^2(\xi_k)].$$

Here, $N_{i,j}^{test}(std)$ is the events corresponding to "fit" in the $\{i,j\}$th bin computed with the standard values of the inputs, "npull" is the number of uncertainties, and σ_k are the uncertainties associated with the kth inputs. ξ_k are the pull variables or nuisance parameters, and they are a measure of how the kth input deviates from its standard value. They describe how the event rates depend on the various sources of systematical errors. In the expression, $c_{i,j}^{k}$ is the change in the expected event spectra when the kth input changes by σ_k. Nuisance systematic parameters are given in Table II. Since we are testing each texture at DUNE, all the "fit values" of the oscillation parameters are as predicted by the texture zero conditions. We have not considered any priors on them in this analysis. Variations of

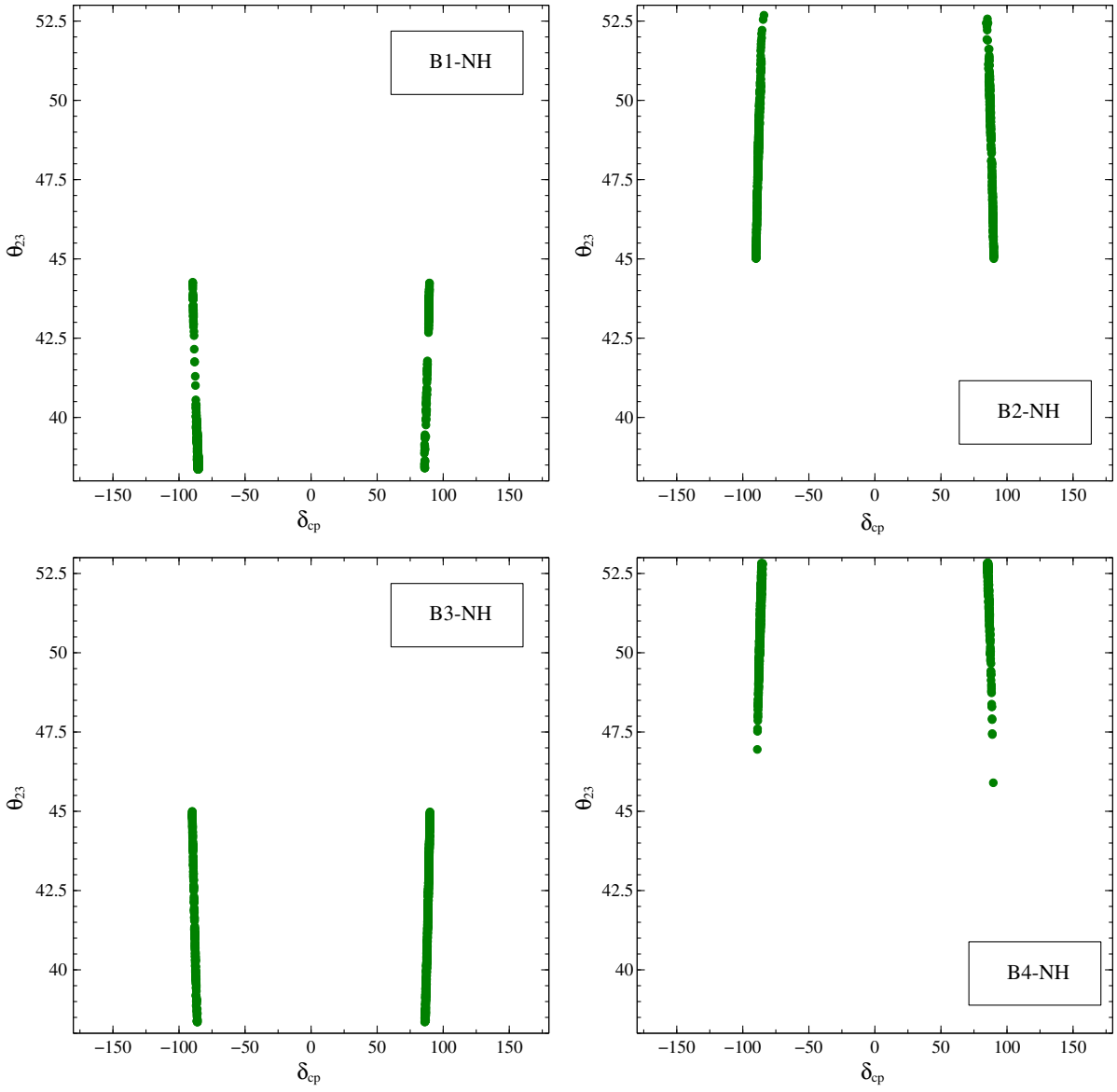

FIG. 6. Neutrino parameters corresponding to two-zero textures for NH.

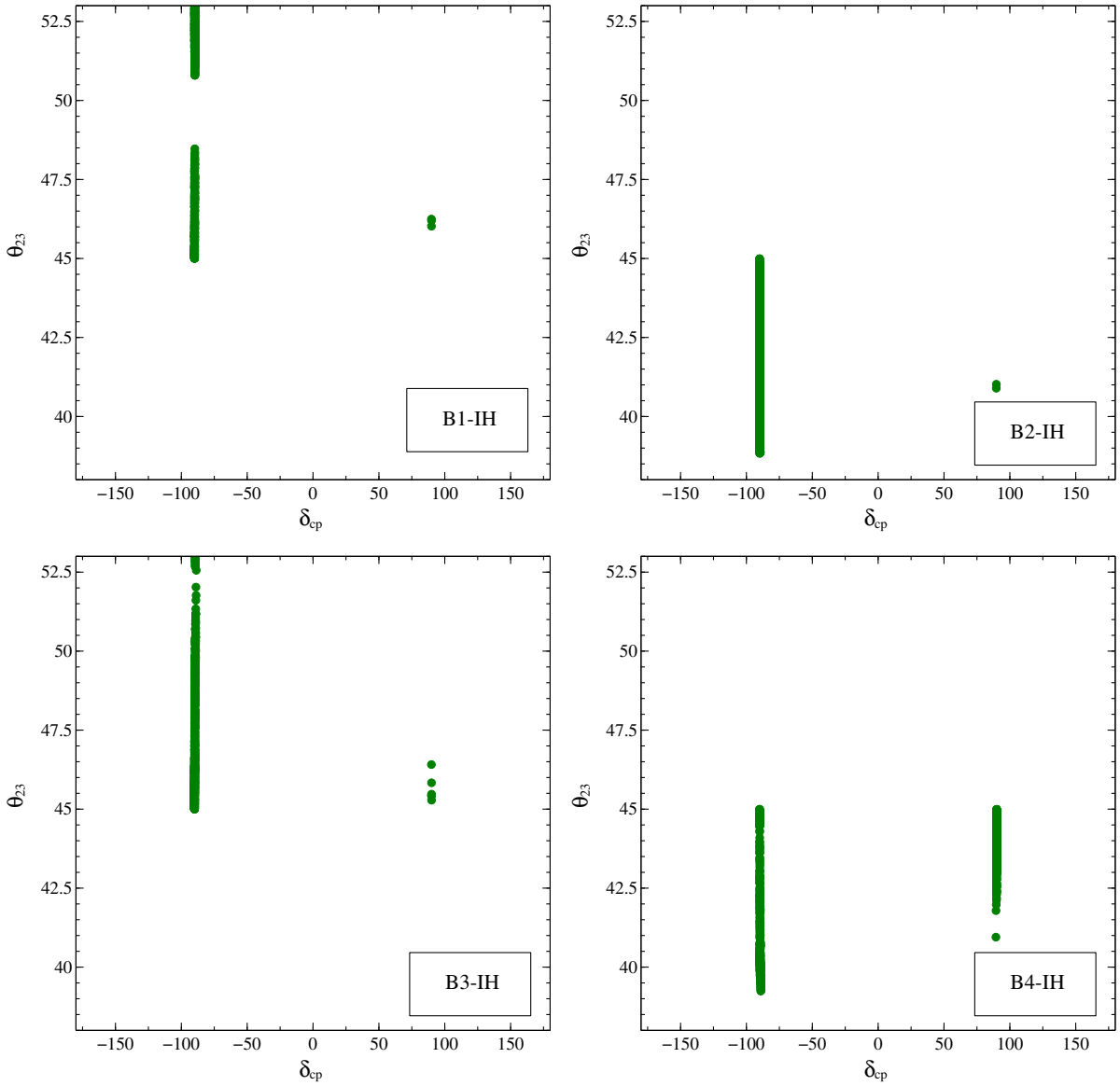

FIG. 7. Neutrino parameters corresponding to two-zero textures for IH.

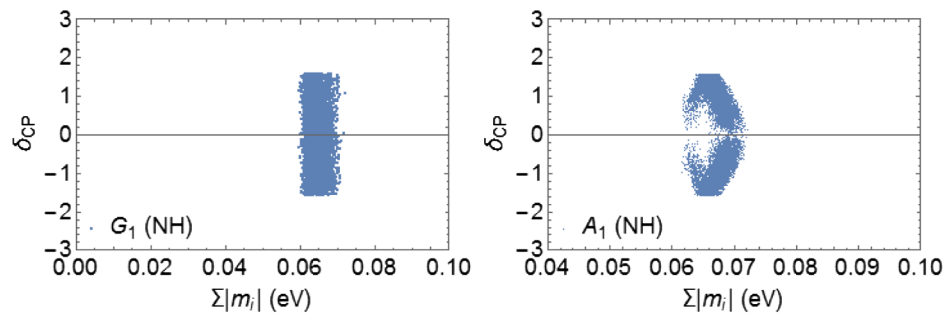

FIG. 8. $\delta_{\rm cp}$ with respect to the sum of absolute neutrino masses for the allowed one- and two-zero textures G_1, A_1 for which $M_{ee} = 0$.

all six neutrino oscillation parameters are taken into account in "fit" according to texture zero conditions.

V. RESULTS AND DISCUSSIONS

A. Allowed texture zero mass matrices

In this section, we discuss the results we obtain for the first part of our analysis—that is, constraining the texture zero mass matrices from the latest experimental bounds on neutrino oscillation parameters, the sum of absolute neutrino masses and the $0\nu\beta\beta$ half-life.

For one-zero texture mass matrices, we numerically solve the two real texture zero equations or the one complex texture zero condition. We solve it for two parameters while randomly varying other parameters in their allowed 3σ range. The lightest neutrino mass is varied in the range 10^{-6}–0.1 eV. For the texture zero mass matrices allowed by neutrino oscillation data alone, we show the corresponding regions of parameter space in the θ_{23}-$\delta_{\rm cp}$ plane in Figs. 1–4 for both NH and IH. It should be noted that, due to there being only two real constraint equations and more unknown neutrino parameters, the one-zero textures are not very predictive. This is obvious from the broad ranges of

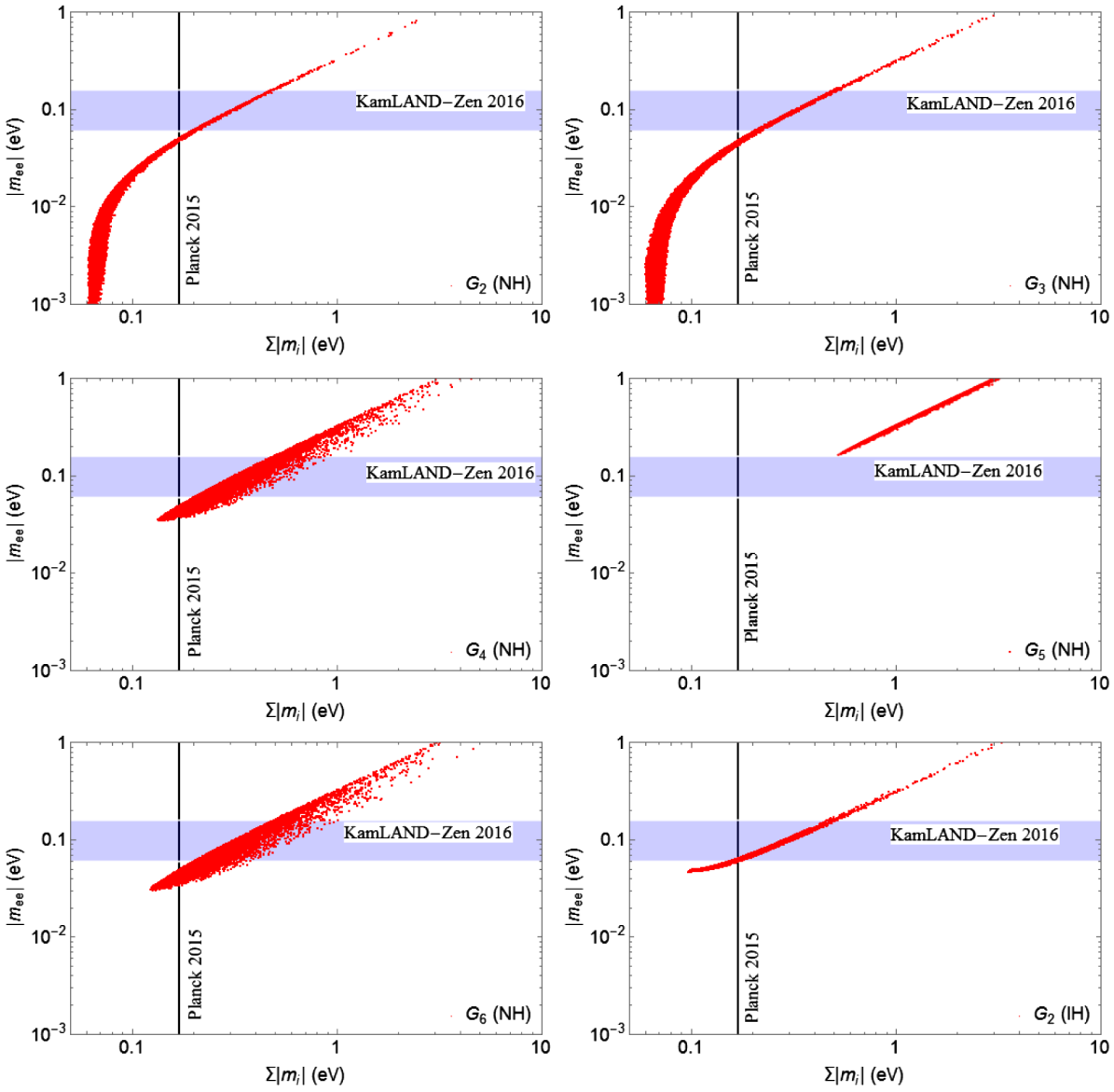

FIG. 9. The contribution to $0\nu\beta\beta$ for one-zero texture mass matrices shown with respect to the sum of absolute neutrino masses. The blue horizontal band corresponds to the 2016 KamLAND-Zen bound $|M_{ee}| < 0.061$–0.165 eV. The vertical solid black line corresponds to the Planck 2015 bound $\sum_i |m_i| < 0.17$ eV.

values allowed in the $(\theta_{23}, \delta_{cp})$ plane. We find that the latest neutrino oscillation data allow all the one-zero texture mass matrices except G_1 with IH.

Similarly, we numerically solve the two complex or four real equations for the two-zero texture mass matrices $A_{1,2}$, $B_{1,2,3,4}$ and extract the resulting parameter space. In this case also, we vary the lightest neutrino mass in the range 10^{-6}–0.1 eV and solve the four real equations numerically in order to evaluate θ_{23}, δ_{cp} along with two Majorana phases. They are shown in Figs. 5–7 for both NH and IH. Since there are four real constraint equations, two-zero texture mass matrices are much more predictive, as can be seen from the narrow range of parameters allowed from the texture zero conditions. We find that the use of the latest 3σ global fit values of solar and reactor mixing angles as well as the two mass-squared differences allow only five two-zero textures with NH and four two-zero textures with IH. This is in contrast with the allowed two-zero texture matrices shown in earlier works [65], as we are using more precise values of neutrino oscillation parameters from the latest global fit data. The allowed textures we have gotten from fitting neutrino oscillation data are the same as the ones obtained in the more recent work [67]. This relatively recent work [67], however, did not include the textures $A_{1,2}$ in their analysis, as they correspond to vanishing amplitude for $0\nu\beta\beta$. Here we include them and find the A_1 texture to be allowed in the case of normal hierarchy. It should be noted that for all these plots in Figs. 1–7, we have not imposed the constraints from the Planck and KamLAND-Zen experiments on the sum of the absolute neutrino masses and the effective light neutrino mass, respectively. At this stage, the viability of the Majorana texture zero mass matrices is studied only in the light of the latest neutrino oscillation data.

After finding the allowed texture zero mass matrices from the requirement of satisfying the latest neutrino oscillation data, we further check their viabilities in the light of cosmology and $0\nu\beta\beta$ bounds mentioned before. Since the textures G_1, A_1 predict vanishing $0\nu\beta\beta$ amplitude, we show δ_{cp} versus the sum of absolute neutrino masses for these two textures in Fig. 8. We find that all the points allowed from neutrino data also obey the Planck 2015 upper bound on $\sum_i |m_i|$. The contributions to $0\nu\beta\beta$ are shown in Figs. 9–11. It is interesting to see from Figs. 9–11 that most of the texture zero mass matrices can saturate the experimental bounds on $0\nu\beta\beta$ as well as the sum of absolute neutrino masses. The two-zero texture mass matrix A_1, however, predicts $\sum_i |m_i|$ far below the

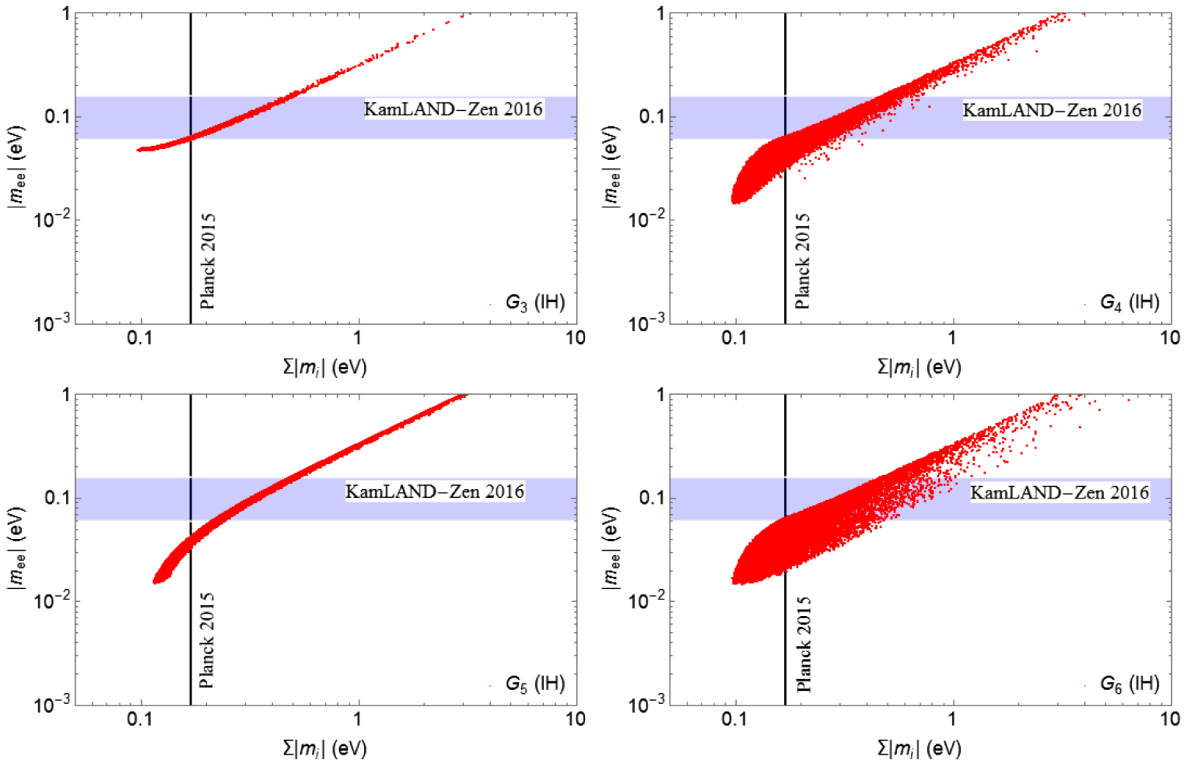

FIG. 10. The contribution to $0\nu\beta\beta$ for one-zero texture mass matrices shown with respect to the sum of absolute neutrino masses. The blue horizontal band corresponds to the 2016 KamLAND-Zen bound $|M_{ee}| < 0.061$–0.165 eV. The vertical solid black line corresponds to the Planck 2015 bound $\sum_i |m_i| < 0.17$ eV.

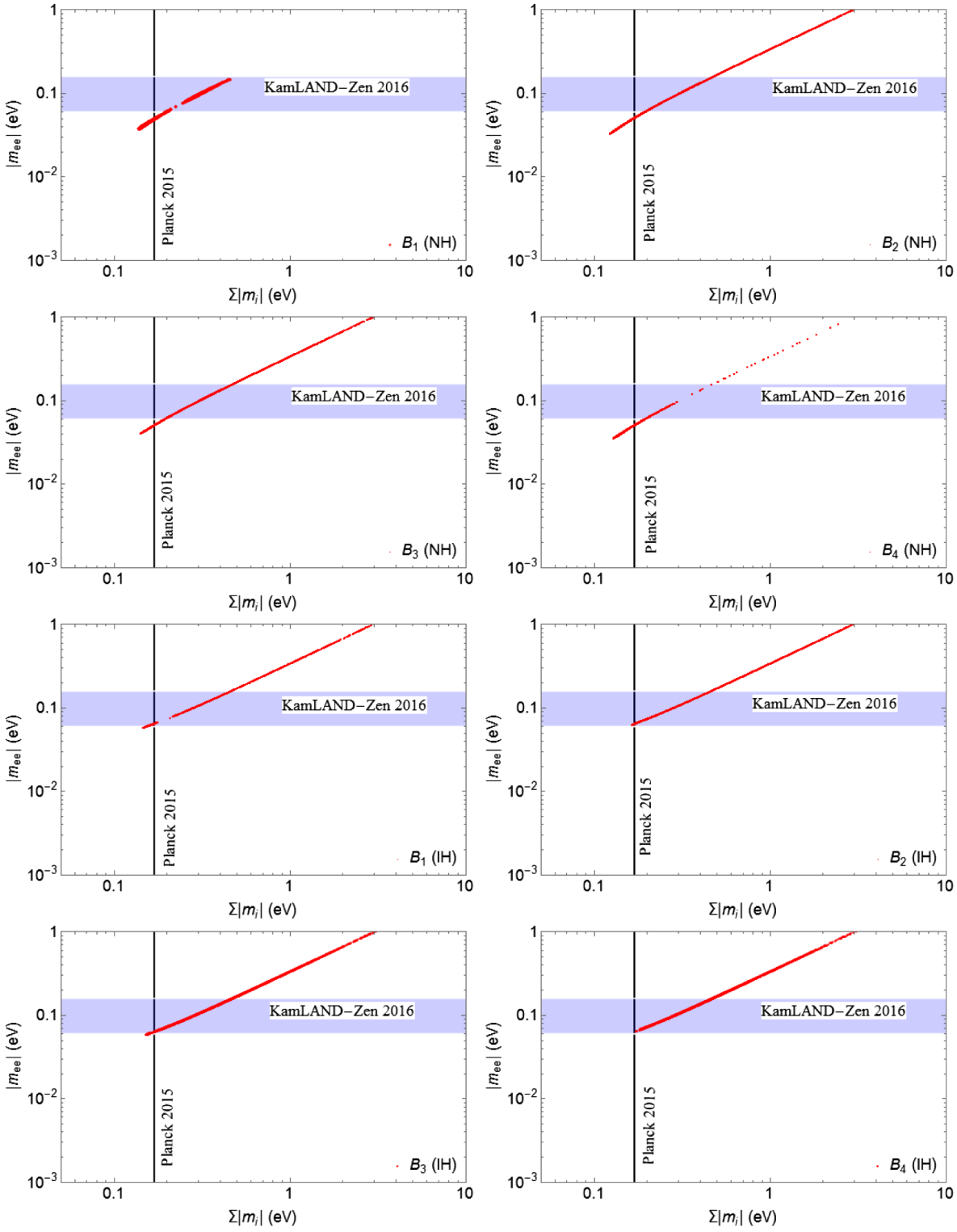

FIG. 11. The contribution to $0\nu\beta\beta$ for two-zero texture mass matrices shown with respect to the sum of absolute neutrino masses. The blue horizontal band corresponds to the 2016 KamLAND-Zen bound $|M_{ee}| < 0.061$–0.165 eV. The vertical solid black line corresponds to the Planck 2015 bound $\sum_i |m_i| < 0.17$ eV.

Planck 2015 bound. We find that one texture zero mass matrix belonging to previously allowed one-zero texture mass matrices becomes disallowed after incorporating these additional constraints. This is namely the G_5 texture with normal hierarchy, as seen from Fig. 9. If we consider the most conservative KamLAND-Zen bound corresponding to the lowermost value of $|M_{ee}|$ in the blue band shown in Figs. 9–11, then two texture zero mass matrices belonging to previously allowed two-zero texture mass matrices become disallowed. They are namely B_2 and B_4, with inverted hierarchy, as seen from Fig. 11. In fact, the B_4 texture with inverted hierarchy is disallowed from the Planck 2015 bound, as seen from the same Fig. 11. Thus, all the two-zero texture mass matrices with NH studied in this work are allowed except A_2, and three such texture zero matrices with IH, namely $B_{1,2,3}$, are allowed. In our subsequent analysis from the DUNE point of view, we will consider these allowed texture zero mass matrices only.

We finally summarize our results from the first part of our analysis in Tables IV and V for one-zero and two-zero texture mass matrices, respectively.

TABLE IV. Summary of results for one-zero texture with inverted and normal hierarchy. The symbol ✓ (×) is used when the particular texture zero mass matrix is (not) consistent with the respective experimental bound.

Patterns	Neutrino data IH (NH)	$0\nu\beta\beta$ bound IH (NH)	Planck bound IH (NH)
G_1	×(✓)	×(✓)	×(✓)
G_2	✓(✓)	✓(✓)	✓(✓)
G_3	✓(✓)	✓(✓)	✓(✓)
G_4	✓(✓)	✓(✓)	✓(✓)
G_5	✓(✓)	✓(×)	✓(×)
G_6	✓(✓)	✓(✓)	✓(✓)

TABLE V. Summary of results for two-zero texture with inverted and normal hierarchy. The symbol ✓ (×) is used when the particular texture zero mass matrix is (not) consistent with the respective experimental bound. A ✓ in red means that the particular texture is only marginally allowed due to the broad band of the upper bound on M_{ee} from the $0\nu\beta\beta$ experiment.

Patterns	Neutrino data IH (NH)	$0\nu\beta\beta$ bound IH (NH)	Planck bound IH (NH)
A_1	×(✓)	×(✓)	×(✓)
A_2	×(×)	×(×)	×(×)
B_1	✓(✓)	✓(✓)	✓(✓)
B_2	✓(✓)	✓(✓)	✓(✓)
B_3	✓(✓)	✓(✓)	✓(✓)
B_4	✓(✓)	✓(✓)	×(✓)

B. Probe of allowed textures at DUNE

In this section, we present our results. We have tested two possible texture zero mass matrices at DUNE—namely, one-zero and two-zero. Each set of textures is tested for both the hierarchies.

In Fig. 12, we show the exclusion of G1, G2, G3, G4, and G6 textures (generated assuming true NH), while in Fig. 13, the allowed/exclusion regions are shown at DUNE in θ_{23}-$\delta_{\rm cp}$ parameter space. The solid green (blue) line corresponds to true $\theta_{23} = 41.6°(48.4°)$, i.e. θ_{23} in the LO (HO); and the red line corresponds to maximal θ_{23}, i.e. $\theta_{23} = 45°$. For each true $\delta_{\rm cp}$, the grey band shows the minimum and maximum of $\chi^2_{\rm min}$ corresponding to the variation of θ_{23} in its 3σ allowed range. In the cases of G1, G2, and G3, only a small portion of the grey band lies above the 5σ C.L., while for the G4 and G6 textures, a large fraction of $\chi^2_{\rm min}$ lies above 5σ. All the region that lies above the 5σ (3σ) black line is excluded at 5σ (3σ). So for most of the true θ_{23}, DUNE can exclude G4 and G6 at the 5σ C.L. for all true $\delta_{\rm cp}$. For the three special cases, we see that except for $\theta_{23} = 41.6°$ in G6-NH, DUNE cannot exclude these textures at 5σ for almost all true $\delta_{\rm cp}$. But for $\theta_{23} = 41.6°$, DUNE can exclude G6-NH at 5σ for some of the true $\delta_{\rm cp}$ except for a small fraction around $\delta_{\rm cp} = 0$. The contours shown in Fig. 13 are defined by $\chi^2 > 4\,(9)$, which corresponds to the 2σ (3σ) C.L. So, for a given texture and for a given set of true θ_{23} and $\delta_{\rm cp}$, if $\chi^2 > 4\,(9)$, then we can say that the texture can be excluded at the 2σ (3σ) C.L. It is observed from the contour plots in Fig. 13 that DUNE can exclude the G4 (G6) texture in the NH mode approximately for all true $\delta_{\rm cp}$ if true $\theta_{23} > 48.5°$ ($\theta_{23} < 43.5°$) at the 3σ C.L. It is difficult to draw such concluding remarks for G1, G2, and G3, as most of the θ_{23}-$\delta_{\rm cp}$ parameter space is allowed at the $2\sigma/3\sigma$ C.L., as seen from the contour plot in Fig. 12.

In Figs. 14 and 15, we show our results for G2, G3, G4, G5, and G6 textures, assuming true IH. Here also, the green (blue) line represents the best-fit value of $\theta_{23} = 40.0°(50.0°)$ in the LO (HO), and the red line corresponds to maximal θ_{23}, i.e. $\theta_{23} = 45°$. The predictivity of these textures is less, as most of the θ_{23}-$\delta_{\rm cp}$ parameter space is allowed at 3σ. But DUNE can exclude G2 and G3 at 3σ for any θ_{23} at the CP-conserving values of $\delta_{\rm cp}$, while G4, G5, and G6 are excluded for $\delta_{\rm cp} = \pm\pi$ at 3σ for all θ_{23}.

In Fig. 16, we present our results for the two-zero textures A1, B1, B2, B3, and B4, assuming true NH. The behavior of the grey band is very similar to the cases of B1, B2, B3, and B4, and most of the θ_{23}-$\delta_{\rm cp}$ parameter space is excluded at DUNE at 3σ. For $\theta_{23} = 41.6°$, DUNE can exclude B1, B2, and B4 at 3σ for all true $\delta_{\rm cp}$. Similarly, B1 and B3 are possible to exclude at 3σ for all $\delta_{\rm cp}$ if $\theta_{23} = 48.4$. As seen from the contour plots in Fig. 17, B1 is more predictive compared to all other two-zero textures in the NH mode, as most of the θ_{23}-$\delta_{\rm cp}$ parameter space is

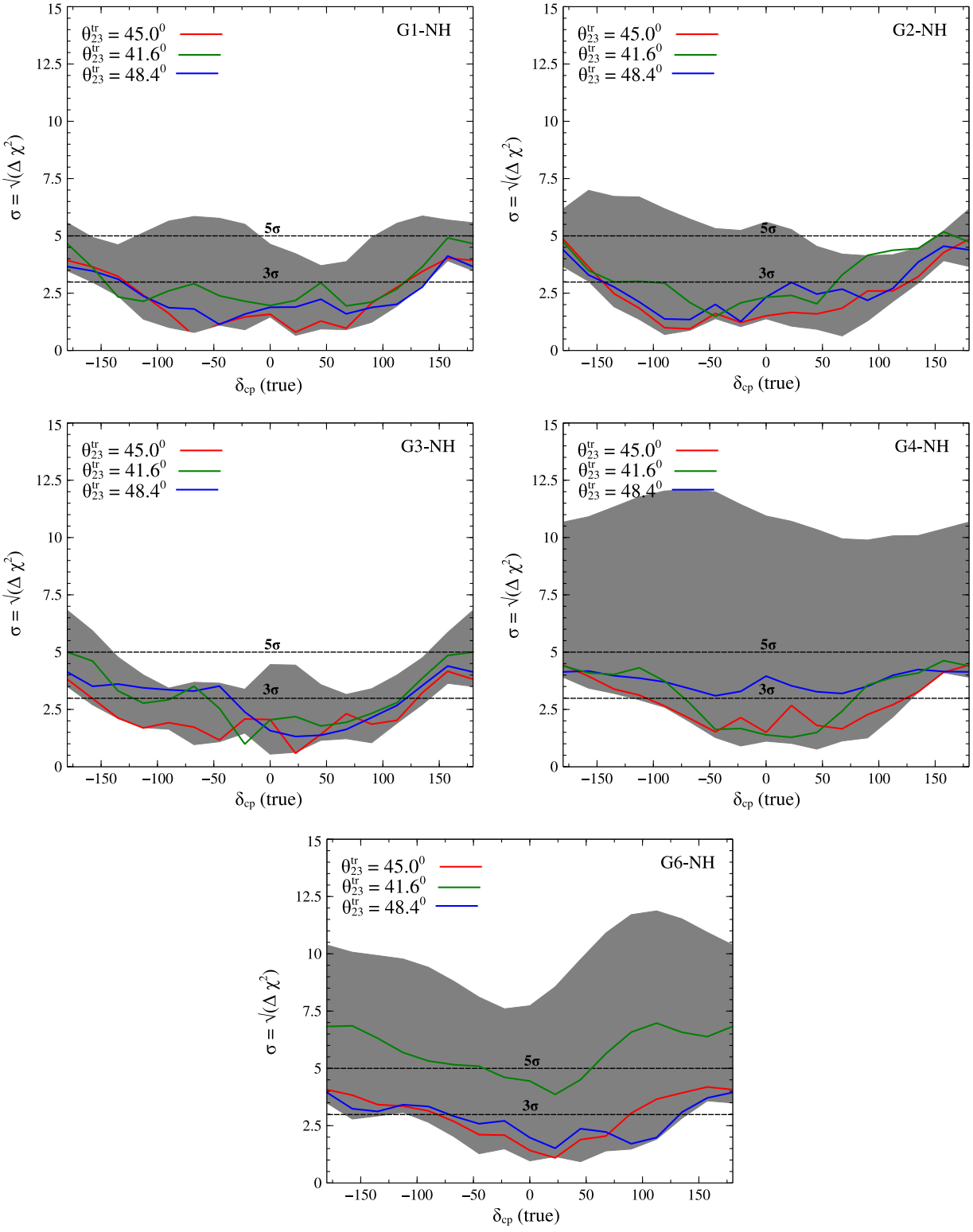

FIG. 12. The exclusion of different one-zero textures at DUNE, assuming NH as the true hierarchy. The grey band represents the full variation of θ_{23} in its 3σ allowed range. The green, blue, and red plots corresponds to three different choices of θ_{23}: i.e. the green plot is for the best-fit value of θ_{23} in the LO, while the blue plot is for θ_{23} in the HO. The red plot is for maximal θ_{23}.

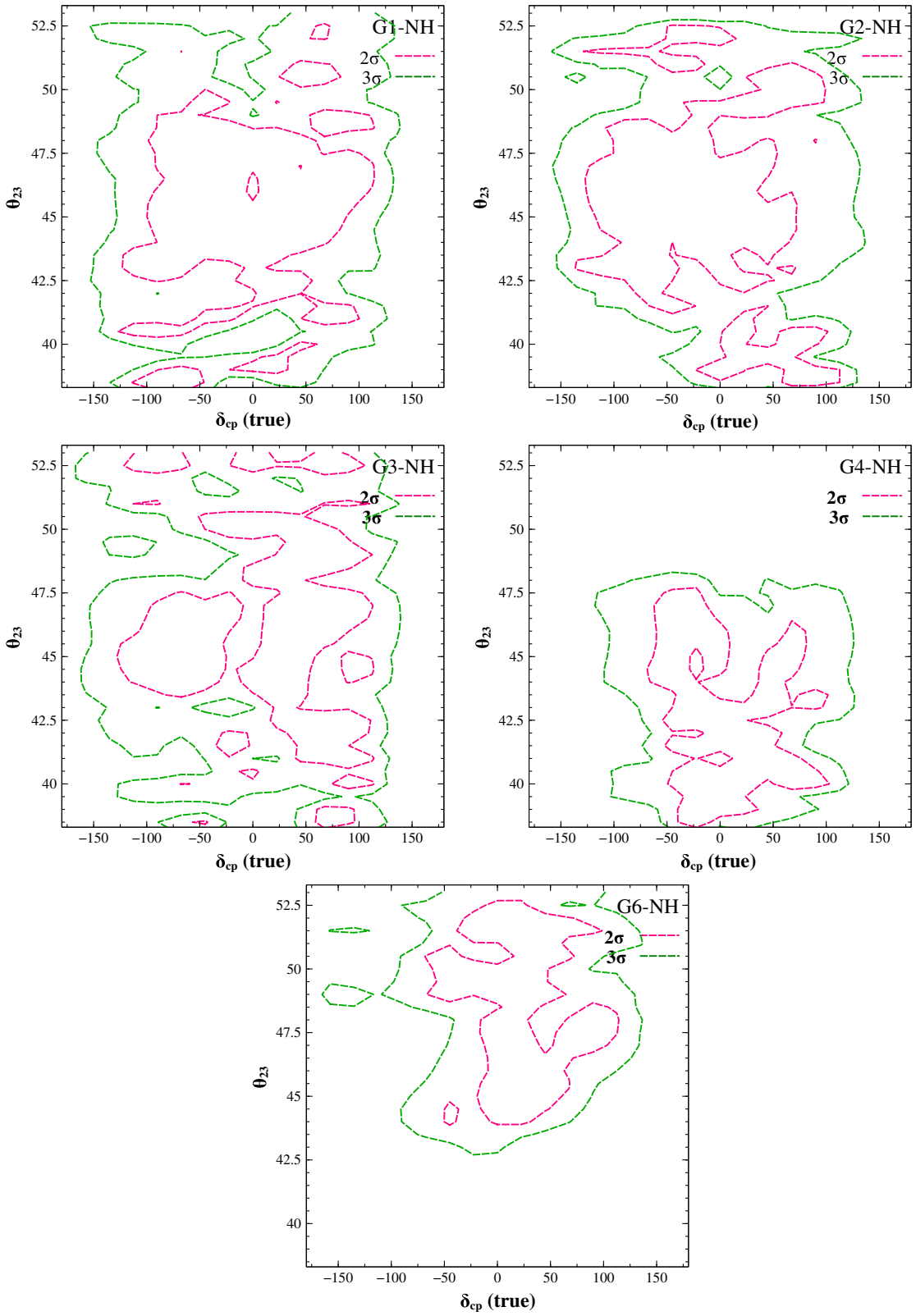

FIG. 13. In the contour plots, we show the allowed regions corresponding to different one-zero textures in NH mode. The green (red) dotted line represents the 3σ (2σ) contour at 1 d.o.f.

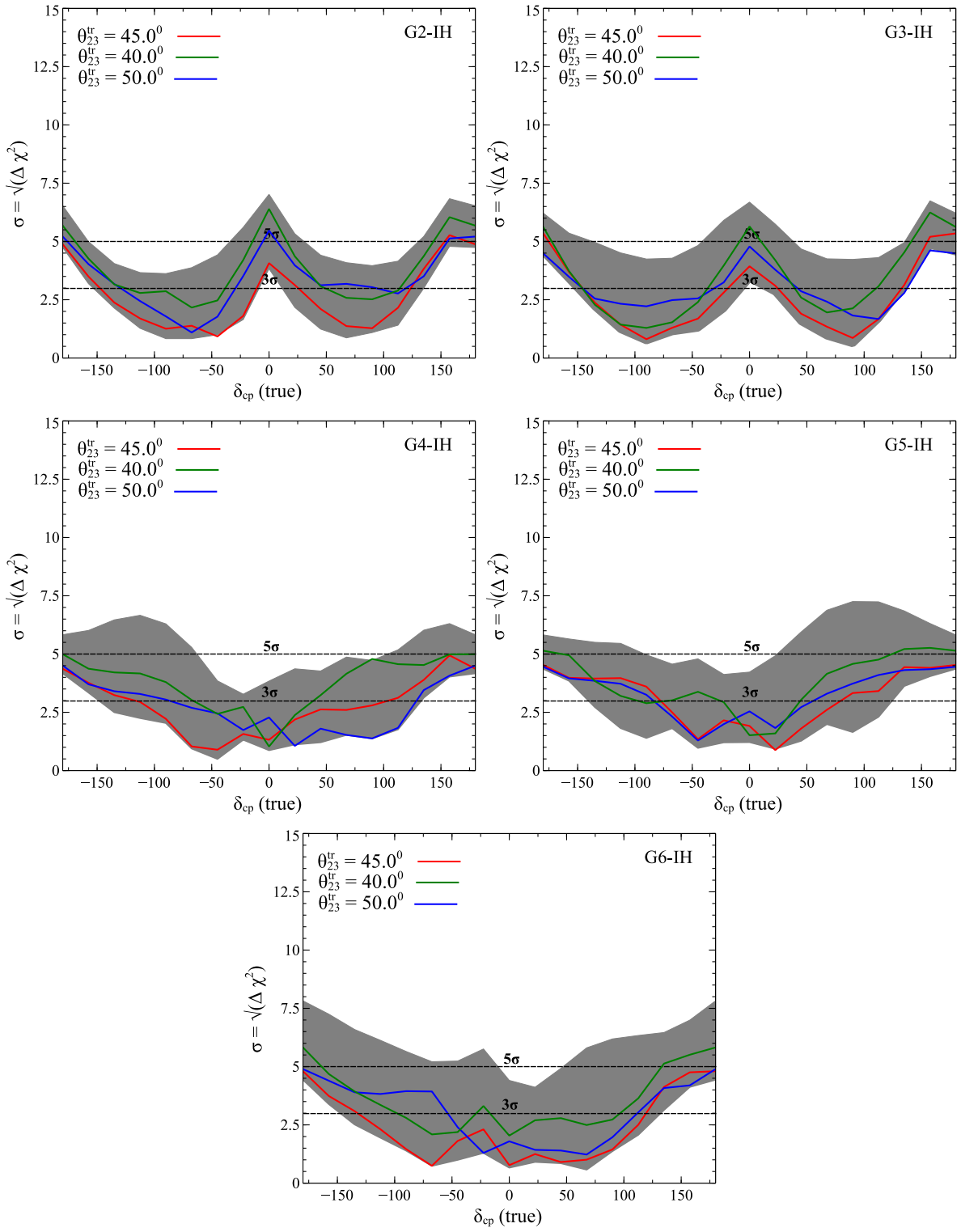

FIG. 14. The exclusion of different one-zero textures at DUNE, assuming IH as the true hierarchy. The grey band represents the full variation of θ_{23} in its 3σ allowed range. The green, blue, and red plots correspond to three different choices of θ_{23}: i.e. the green plot is for the best-fit value of θ_{23} in the LO, while the blue plot is for θ_{23} in the HO. The red plot is for maximal θ_{23}.

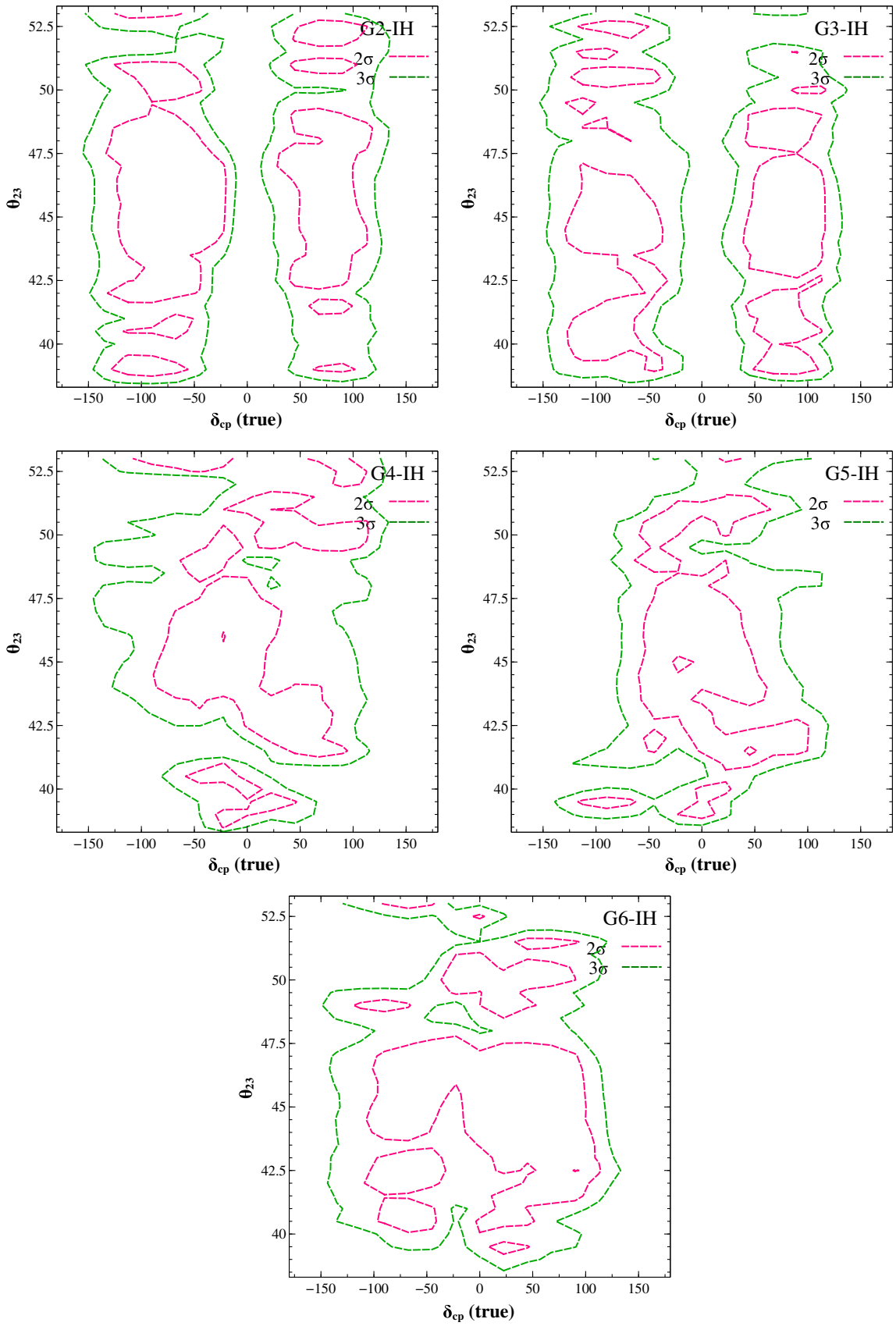

FIG. 15. In the contour plots, we show the allowed regions corresponding to different one-zero textures in IH mode. The green (red) dotted line represents the 3σ (2σ) contour at 1 d.o.f.

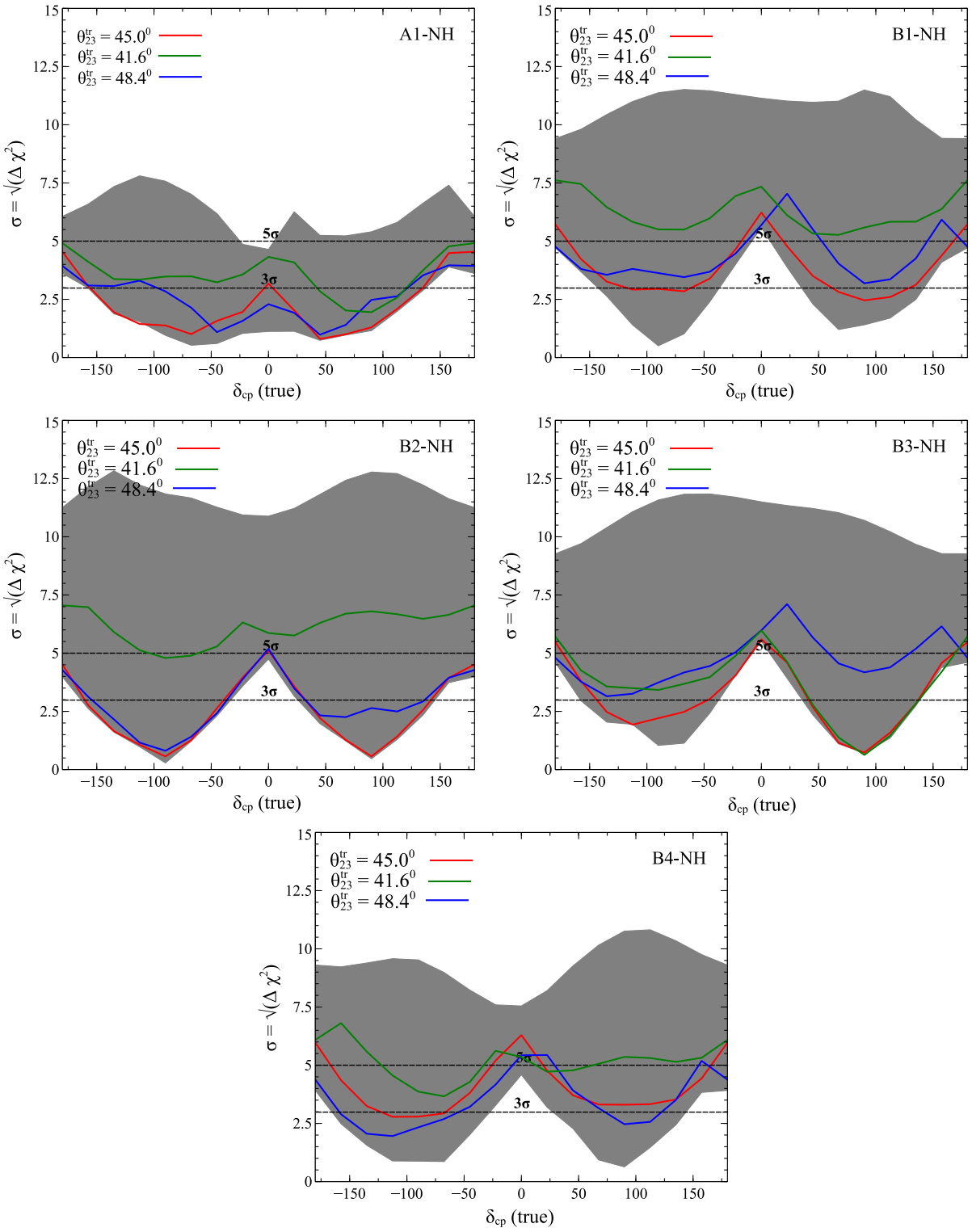

FIG. 16. The exclusion of different two-zero textures at DUNE, assuming NH as the true hierarchy. In the upper panel, the grey band represents the full variation of θ_{23} in its 3σ allowed range. The green, blue, and red plots correspond to three different choices of θ_{23}: i.e. the green plot is for the best-fit value of θ_{23} in the LO, while the blue plot is for θ_{23} in the HO. The red plot is for maximal θ_{23}.

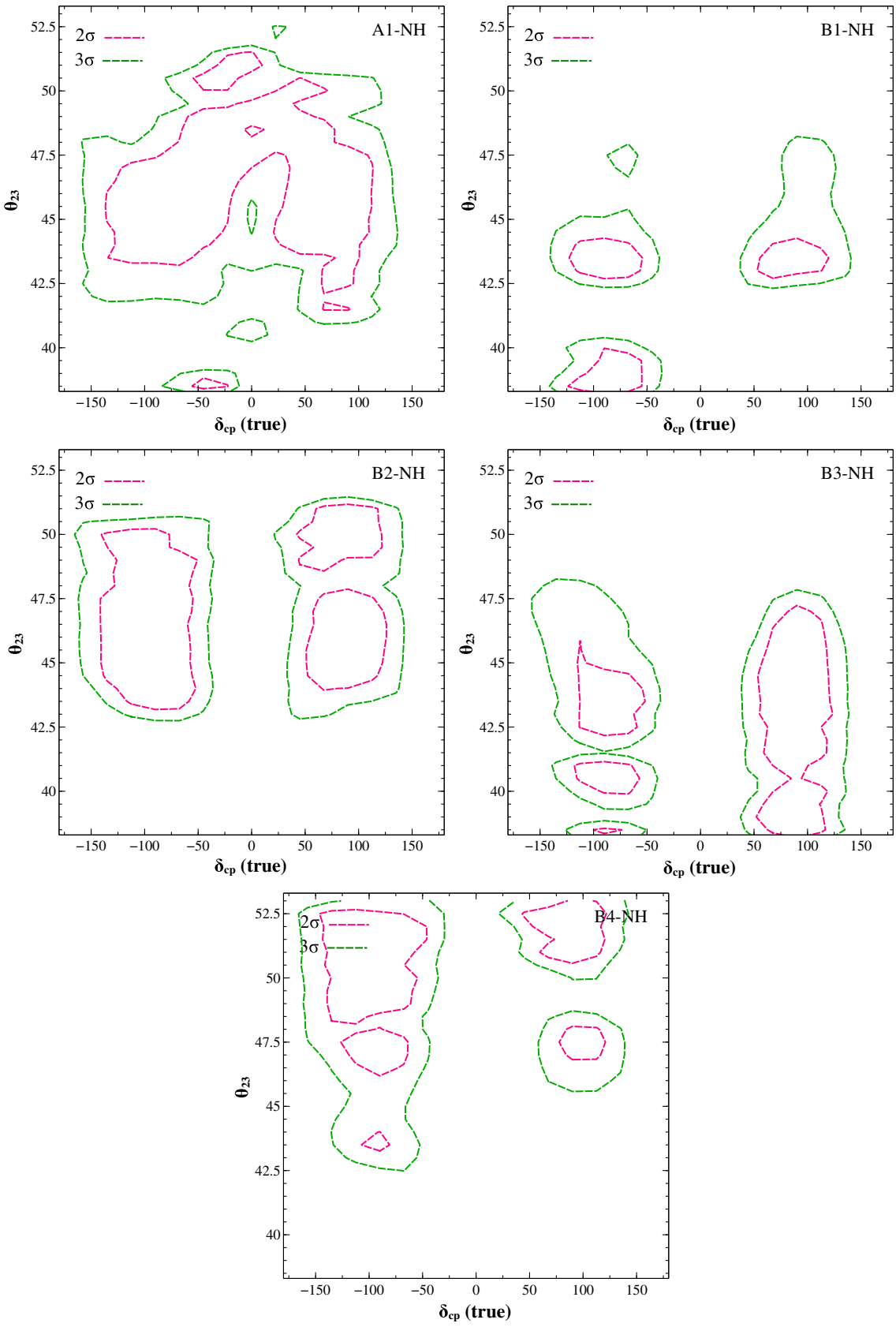

FIG. 17. In the contour plots, we show the allowed regions corresponding to different two-zero textures in the NH mode. The green (red) dotted line represents the 3σ (2σ) contour at 1 d.o.f.

excluded at 3σ. For almost any θ_{23} in HO, DUNE can exclude B1 for all true values of δ_{cp} at 2σ, as seen from Fig. 17. For any $\theta_{23} > 51.5°$ and $\theta_{23} < 42.5°$, DUNE can exclude B2 for all true δ_{cp} at 3σ C.L.. Similarly, DUNE can exclude both B3 and B4 for all true δ_{cp} at 3σ, if $\theta_{23} > 48.5°$ and $\theta_{23} < 42.5°$, respectively. A1 is less predictive, as it allows most of the θ_{23}-δ_{cp} parameter space at 3σ. Except for A1, all other two-zero textures in the NH mode are excluded at DUNE for the *CP*-conserving values almost at the 5σ C.L. (see Fig. 16).

In Figs. 18 and 19, we have shown our results for the B1, B2, and B3 textures, assuming IH as the true hierarchy. It is observed that B1 and B2 textures can be excluded at DUNE for all true δ_{cp} in the upper half-plane (UHP, δ_{cp} from 0° to 180°) for any values of θ_{23} at the 5σ C.L. If $\theta_{23} = 40.0°$, then DUNE can exclude both B1 and B3 at 5σ, irrespective of any true δ_{cp}. For this θ_{23}, DUNE can exclude B2 for all δ_{cp} in the UHP at 5σ. Similarly, for maximal θ_{23}, both B1 and B2 can be excluded at 5σ in the UHP. If true $\theta_{23} = 50.0°$, then DUNE has the potential to exclude both B1 and B2 at 3σ for all true δ_{cp}, and it can rule out B3 at 5σ for all true δ_{cp} in the UHP. We observe from Fig. 19 that most of the θ_{23}-δ_{cp} parameter space is ruled out at 3σ in the cases of B1 and B2. All θ_{23}'s are excluded at 3σ for all true δ_{cp} in the UHP. In the lower half-plane of δ_{cp} (LHP, δ_{cp} from $-180°$ to 0°), DUNE can exclude both B1 and B2 at 3σ if $\theta_{23} < 43.0°$ and $\theta_{23} > 48°$, respectively. DUNE can exclude B3 at 3σ for all true δ_{cp} if nature chooses θ_{23} such that $\theta_{23} < 42.5°$. DUNE allows B3 almost for all δ_{cp} except some fractions around the *CP*-conserving values. All these textures in IH mode are excluded at DUNE for the *CP*-conserving values at 5σ, irrespective of any true θ_{23}.

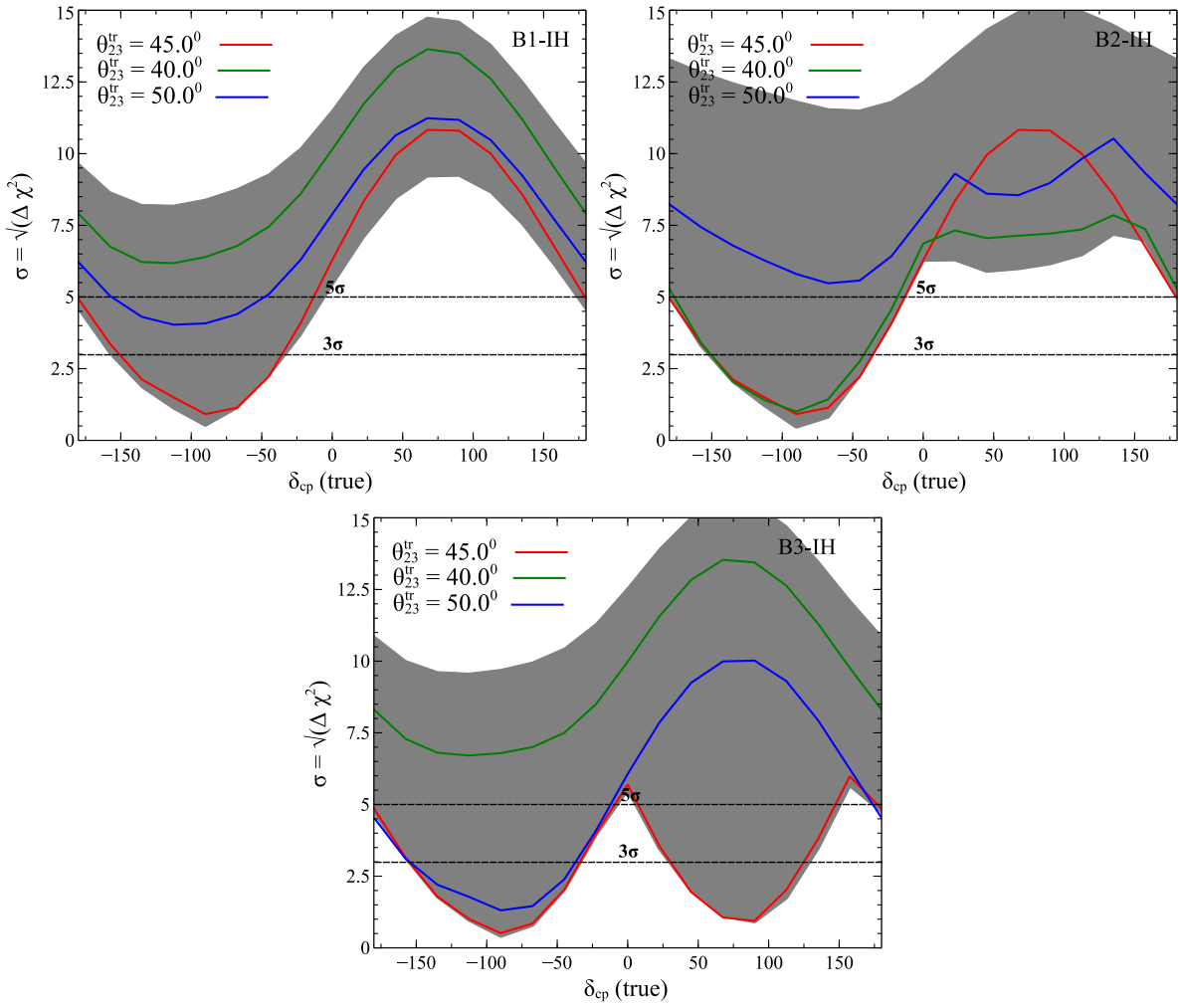

FIG. 18. The exclusion of different two-zero textures at DUNE, assuming IH as the true hierarchy. In the upper panel, the grey band represents the full variation of θ_{23} in its 3σ allowed range. The green, blue, and red plots correspond to three different choices of θ_{23}: i.e. the green plot is for the best-fit value of θ_{23} in the LO, while the blue plot is for θ_{23} in the HO. The red plot is for maximal θ_{23}.

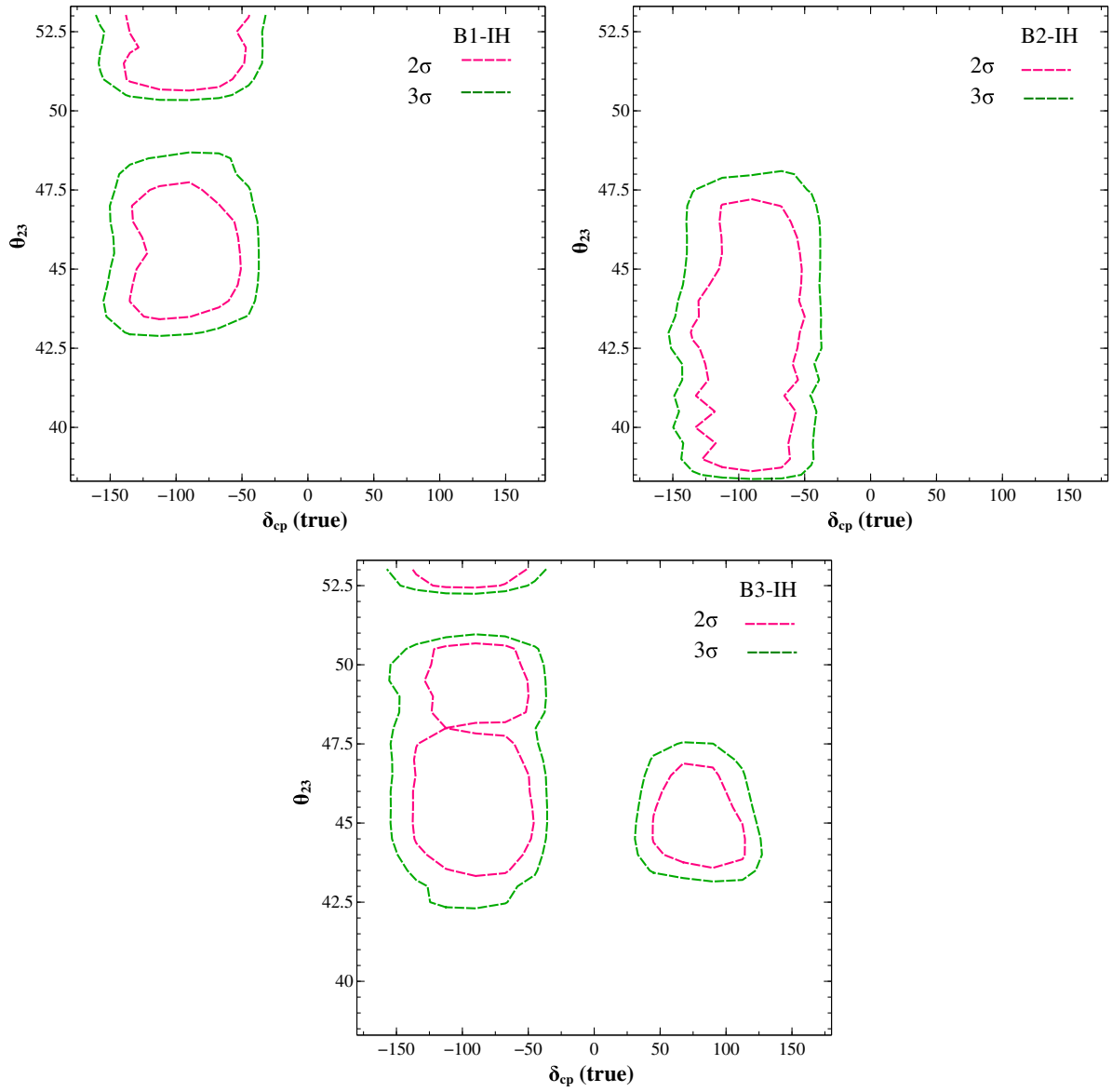

FIG. 19. In the contour plots, we show the allowed regions corresponding to different two-zero textures in the IH mode. The green (red) dotted line represents the 3σ (2σ) contour at 1 d.o.f.

DUNE is an upcoming experiment, and hence it is very much important to ask the following question: if nature chooses one of these mass textures—i.e. the true values of θ_{23} and $\delta_{\rm cp}$ lie in the range restricted by the texture—then how DUNE can exclude the present oscillation scenario? To answer that question, we choose the discrete data sets (from Figs. 1–7) which are an outcome of a constraint equation from the textures as the "data" or "true values," and in the "fit," we consider the standard oscillation scenario—i.e. we vary $\delta_{\rm cp}$ and θ_{23} in their 3σ allowed range. Then χ^2 is calculated between the "data" and "fit." We show the results (from Figs. 20–23) as a function of true θ_{23} and true $\delta_{\rm cp}$. If for a particular choice of true parameters, all test values give $\chi^2 > 4$ ($\chi^2 > 9$), then we can say that the standard oscillation scenario can be excluded at the 2σ (3σ) C.L. In θ_{23}-$\delta_{\rm cp}$ (true) parameter space, a point has been marked by a magenta star if for that point $\chi^2_{\rm min}$ is greater than 4 but less than 9. All blue triangles represent the points which give $\chi^2_{\rm min} > 9$. So for all colored points, we can say that DUNE can exclude the standard scenario at a 2σ C.L. DUNE can exclude the standard scenario at a 3σ C.L. only for the blue points.

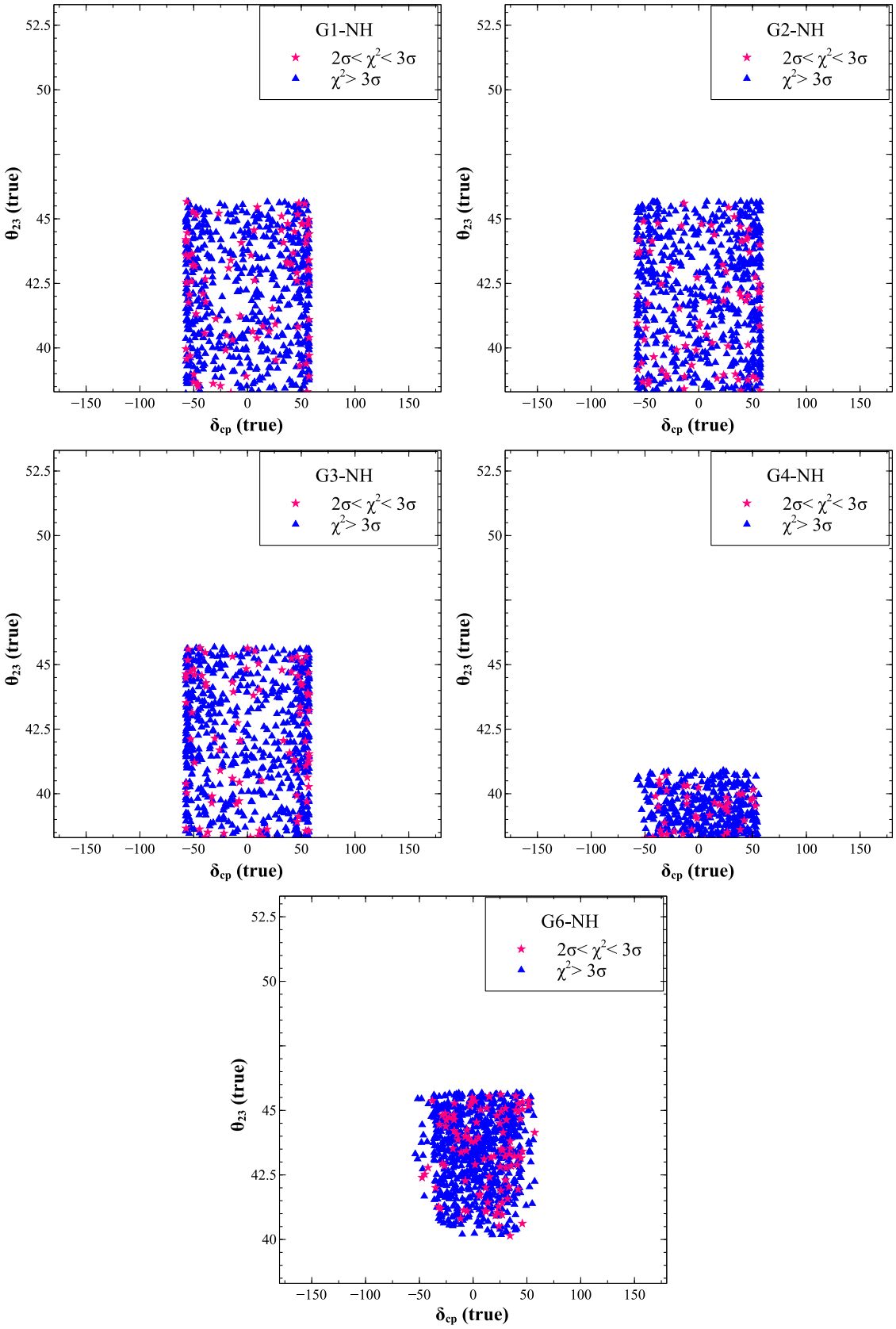

FIG. 20. Region of the $\theta_{23} - \delta_{cp}$ parameter space for which DUNE can establish one-zero texture against the present oscillation scenario for assumed true NH.

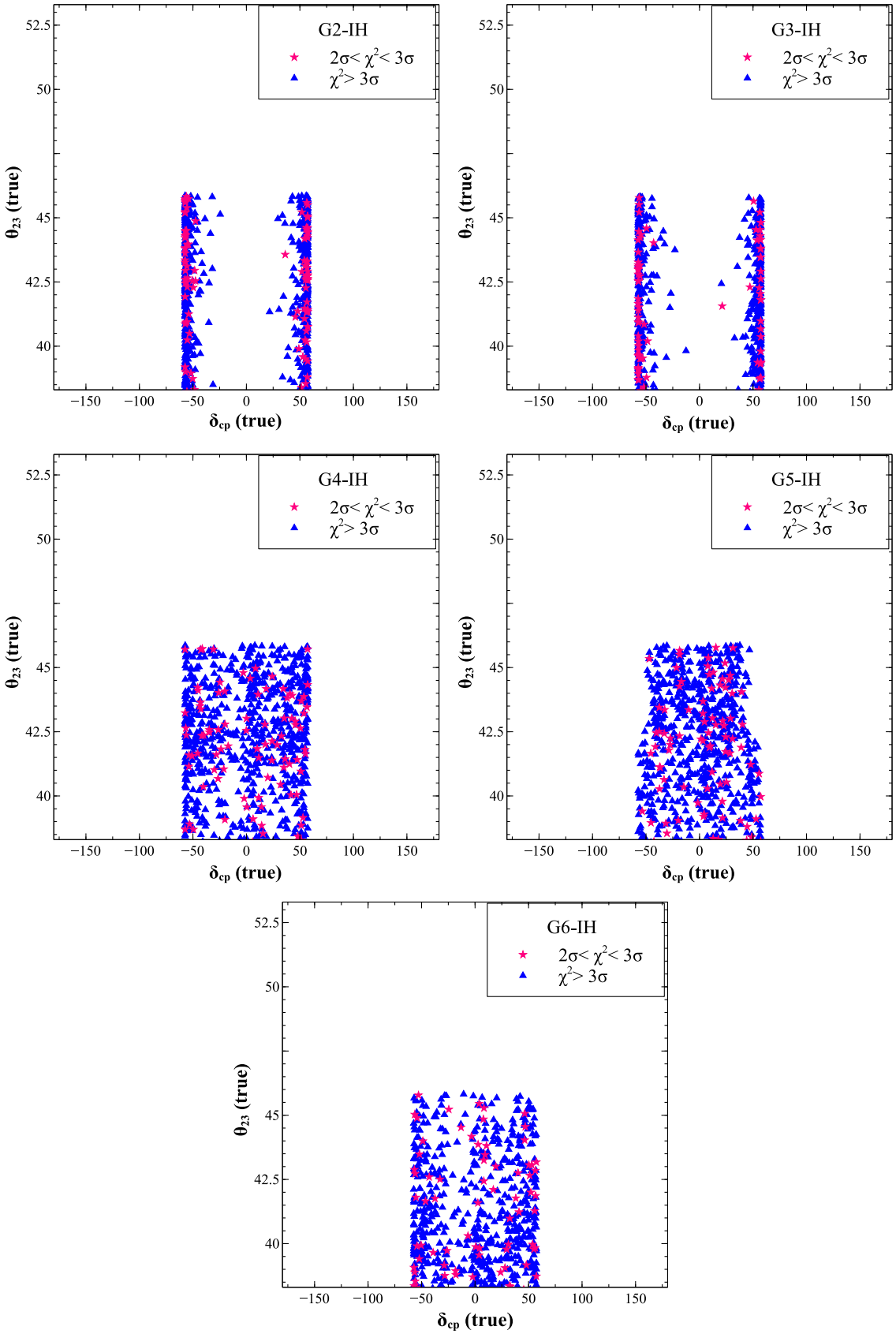

FIG. 21. Region of the θ_{23}-δ_{cp} parameter space for which DUNE can establish one-zero texture against the present oscillation scenario for assumed true IH.

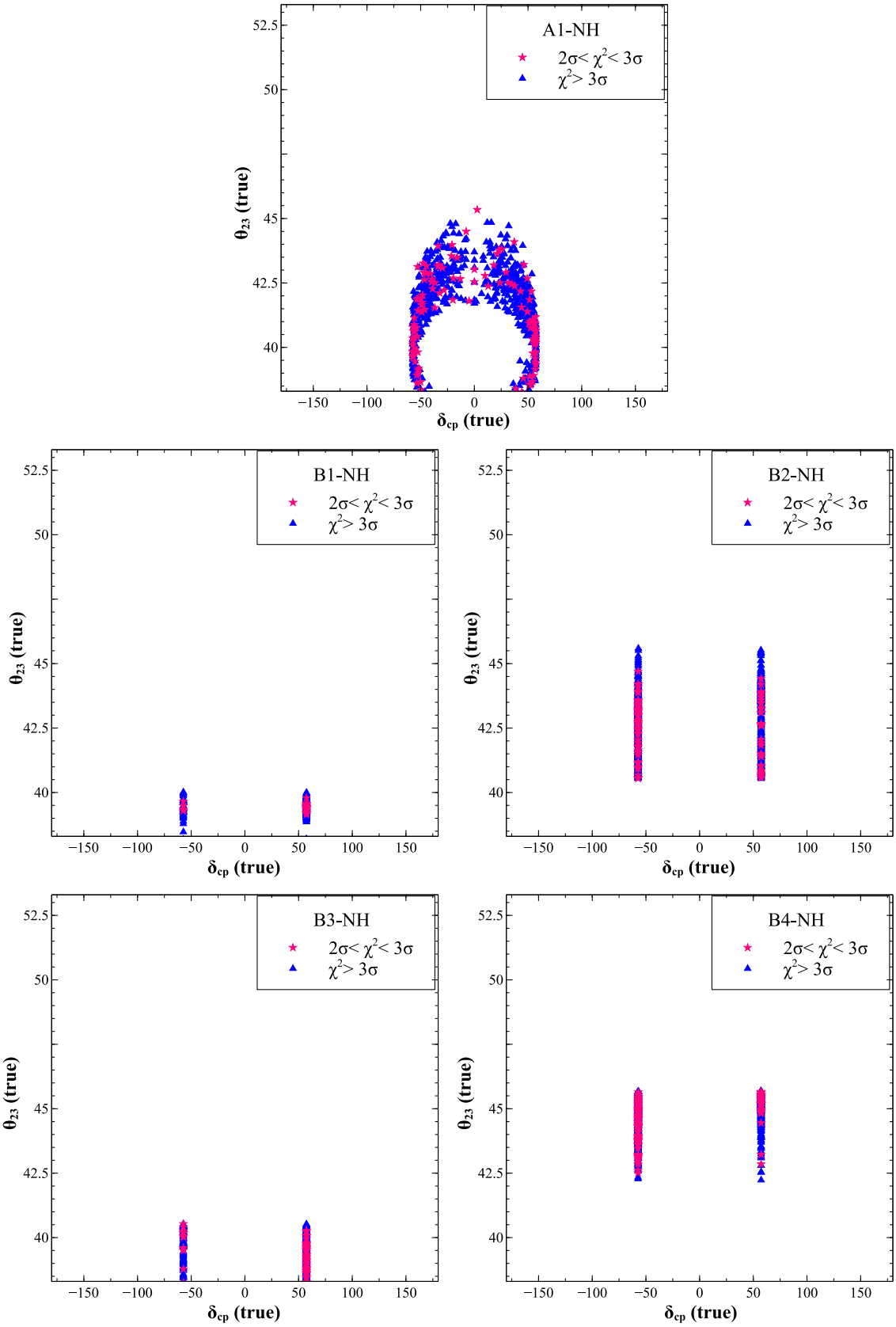

FIG. 22. Region of the θ_{23}-δ_{cp} parameter space for which DUNE can establish two-zero texture against the present oscillation scenario for assumed true NH.

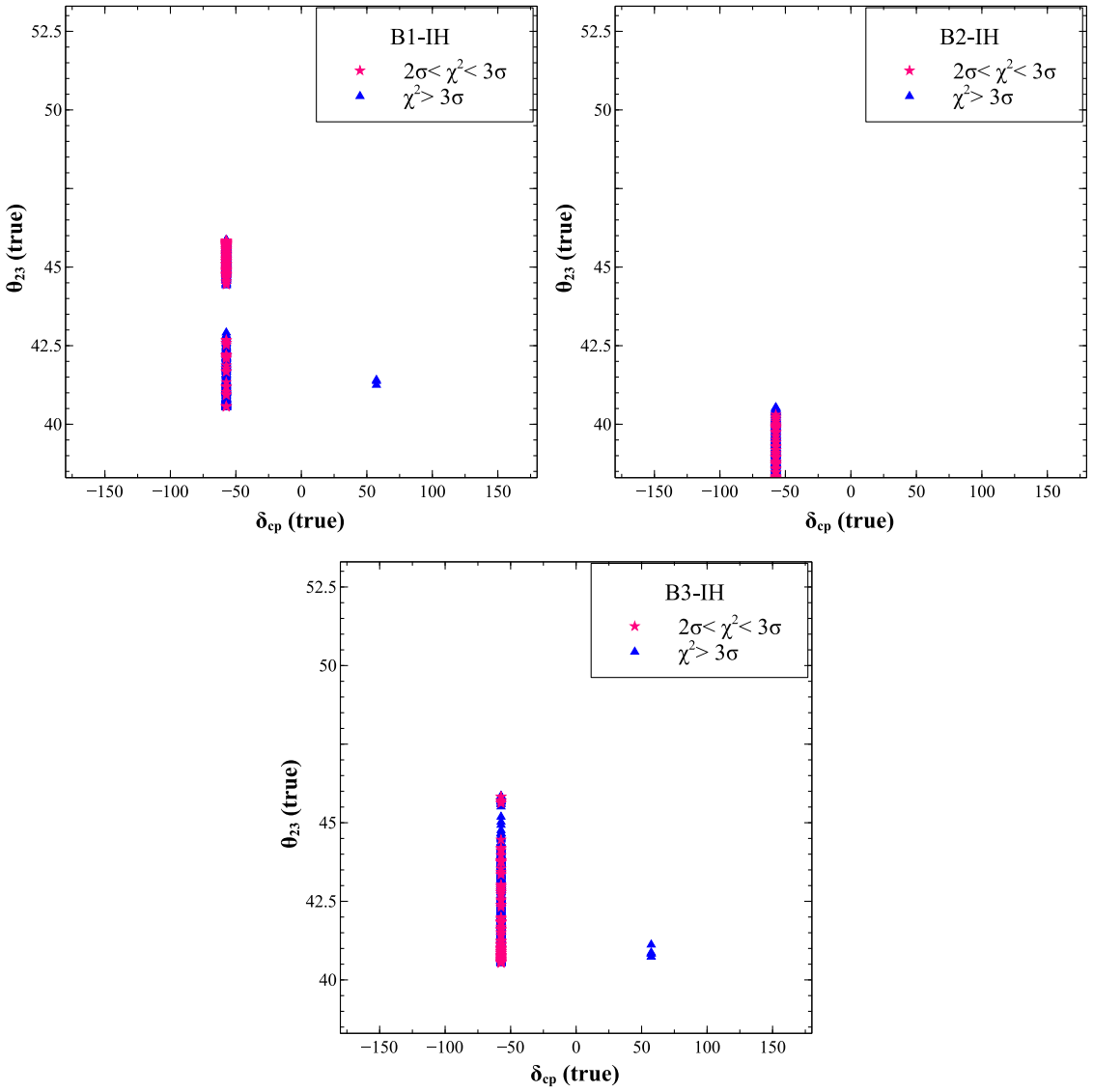

FIG. 23. Region of the θ_{23}-δ_{cp} parameter space for which DUNE can establish two-zero texture against the present oscillation scenario for assumed true IH.

VI. CONCLUSIONS

To conclude, in this work, we perform a phenomenological study on one-zero and two-zero textures from DUNE prospective. We first constrain the different possible one-zero and two-zero texture mass matrices from the latest experimental data on oscillation parameters, the sum of the absolute neutrino mass, as well as the lower bound on the half-life of neutrinoless double beta decay. Using the most recent bounds on these parameters, we find that some of the texture zero mass matrices previously shown to be allowed become disfavored or only marginally allowed. The allowed textures—in particular, the two-zero texture mass matrices—also predict the neutrino parameters like θ_{23}, $\delta_{\rm cp}$, etc. to lie in a very specific range that can be probed in long baseline neutrino experiments like DUNE.

In the second part of our work, we have studied the capability of DUNE to probe different mass textures once it takes data. We have shown our results for both one-zero and two-zero textures for both the hierarchies. Depending on the values of θ_{23} and $\delta_{\rm cp}$ that nature chooses, how DUNE allows or excludes these textures is presented in this work. From the analyses, we have observed that the most of the θ_{23}-$\delta_{\rm cp}$ parameter space is allowed for the one-zero textures in both the hierarchies at 3σ. DUNE excludes the G4 (G6) texture at 3σ almost for all $\delta_{\rm cp}$ if the true $\theta_{23} > 47.5°$ ($\theta_{23} < 44°$) and the assumed true hierarchy is normal. DUNE can exclude G3 at 3σ for any θ_{23} for all the CP-conserving values of $\delta_{\rm cp}$; while G4, G5, and G6 are excluded for $\delta_{\rm cp} = \pm\pi$ at 3σ for assumed true IH. Except for A1, all other two-zero textures are excluded for

CP-conserving values at 4σ, irrespective of θ_{23} and hierarchies. We have observed that these two-zero textures are very interesting from DUNE's prospective, as most of the true θ_{23}-δ_{cp} parameter space is excluded at DUNE. Specially, for any θ_{23} in the HO, DUNE can exclude B1-NH for all true values of δ_{cp} at 3σ. If θ_{23} is such that $\theta_{23} > 51°$ and $\theta_{23} < 43.5°$, then DUNE can rule out B2-NH for all true δ_{cp} at the 3σ C.L. Similarly, if $\theta_{23} > 48°$ ($\theta_{23} < 44°$), DUNE excludes B3-NH (B4-NH) for all true δ_{cp} at 3σ.

Again, for assumed true IH, we have found that B1 and B2 textures can be excluded at DUNE for all true δ_{cp} in the upper half-plane (UHP, δ_{cp} from 0° to 180°) for any values of θ_{23} at 5σ C.L. If nature chooses θ_{23} such that $\theta_{23} < 43.5°$, DUNE can exclude B3 at 3σ for all true δ_{cp}.

From this study, we have observed that irrespective of neutrino mass ordering, DUNE can exclude most of the true θ_{23}-δ_{cp} parameter space of B1 texture and hence restricts B1 more tightly.

Since the texture zero mass matrices can be generated by different flavor symmetry models considered in several earlier works [43–52], possible discrimination of different texture zeros at DUNE studied in this work could also disfavor certain flavor symmetry models leading to some particular textures. Although the new physics sector is not directly affecting the neutrino oscillation probabilities analytically, its presence is indirectly tested by probing the specific neutrino parameters it predicts through a particular texture zero mass matrix. This study can also be extended to other texture zero models like those with a nondiagonal charged lepton mass matrix or those with additional light sterile neutrinos. We are working on these possibilities, which will be presented in an upcoming work [83].

ACKNOWLEDGMENTS

We acknowledge the use of the HRI cluster facility to carry out computations. D. D. thanks Prof. Raj Gandhi for his support, as well as discussions regarding DUNE. He acknowledges the support from Gauhati University and the XII Plan Neutrino Project of the Department of Atomic Energy at HRI to visit Gauhati University and IIT, Guwahati. He also thanks Suprabh Prakash for some useful discussions during his HRI visit.

APPENDIX: LIGHT NEUTRINO MASS MATRIX ELEMENTS

$$M_{ee} = c_{12}^2 c_{13}^2 m_1 + c_{13}^2 s_{12}^2 m_2 e^{i2\alpha} + s_{13}^2 m_3 e^{i2\beta} \tag{A1}$$

$$\begin{aligned} M_{e\mu} = M_{\mu e} = c_{13}(&s_{13}s_{23}m_3 e^{i(\delta_{cp}+2\beta)} \\ &- c_{12}m_1(c_{23}s_{12} + c_{12}s_{13}s_{23}e^{i\delta_{cp}}) \\ &+ s_{12}m_2 e^{i2\alpha}(c_{12}c_{23} - s_{12}s_{13}s_{23}e^{i\delta_{cp}})) \end{aligned} \tag{A2}$$

$$\begin{aligned} M_{e\tau} = M_{\tau e} = c_{13}(&c_{23}s_{13}m_3 e^{i(\delta_{cp}+2\beta)} \\ &- s_{12}m_2 e^{i2\alpha}(c_{23}s_{12}s_{13}e^{i\delta_{cp}} + c_{12}s_{23}) \\ &+ c_{12}m_1(-c_{12}c_{23}s_{13}e^{i\delta_{cp}} + s_{12}s_{23})) \end{aligned} \tag{A3}$$

$$\begin{aligned} M_{\mu\mu} = {} & c_{13}^2 s_{23}^2 m_3 e^{i2(\delta_{cp}+\beta)} + m_1(c_{23}s_{12} + c_{12}s_{13}s_{23}e^{i\delta_{cp}})^2 \\ & + m_2 e^{i2\alpha}(c_{12}c_{23} - s_{12}s_{13}s_{23}e^{i\delta_{cp}})^2 \end{aligned} \tag{A4}$$

$$\begin{aligned} M_{\mu\tau} = M_{\tau\mu} = {} & c_{13}^2 c_{23}s_{23}m_3 e^{i2(\delta_{cp}+\beta)} \\ & + m_1(c_{12}c_{23}s_{13}e^{i\delta_{cp}} - s_{12}s_{23})(c_{23}s_{12} + c_{12}s_{13}s_{23}e^{i\delta_{cp}}) \\ & - m_2 e^{i2\alpha}(c_{23}s_{12}s_{13}e^{i\delta_{cp}} + c_{12}s_{23}) \\ & \times (c_{12}c_{23} - s_{12}s_{13}s_{23}e^{i\delta_{cp}}) \end{aligned} \tag{A5}$$

$$\begin{aligned} M_{\tau\tau} = {} & c_{13}^2 c_{23}^2 m_3 e^{i2(\delta_{cp}+\beta)} + m_2 e^{i2\alpha}(c_{23}s_{12}s_{13}e^{i\delta_{cp}} + c_{12}s_{23})^2 \\ & + m_1(c_{12}c_{23}s_{13}e^{i\delta_{cp}} - s_{12}s_{23})^2 \end{aligned} \tag{A6}$$

[1] S. Fukuda *et al.* (Super-Kamiokande Collaboration), Phys. Rev. Lett. **86**, 5656 (2001); Q. R. Ahmad *et al.* (SNO Collaboration), Phys. Rev. Lett. **89**, 011301 (2002); **89**, 011302 (2002); J. N. Bahcall and C. Pena-Garay, New J. Phys. **6**, 63 (2004); K. Nakamura *et al.*, J. Phys. G **37**, 075021 (2010).
[2] S. Abe *et al.* (KamLAND Collaboration), Phys. Rev. Lett. **100**, 221803 (2008).
[3] K. Abe *et al.* (T2K Collaboration), Phys. Rev. Lett. **107**, 041801 (2011).
[4] Y. Abe *et al.*, Phys. Rev. Lett. **108**, 131801 (2012).
[5] F. P. An *et al.* (DAYA-BAY Collaboration), Phys. Rev. Lett. **108**, 171803 (2012).
[6] J. K. Ahn *et al.* (RENO Collaboration), Phys. Rev. Lett. **108**, 191802 (2012).
[7] P. Adamson *et al.* (MINOS Collaboration), Phys. Rev. Lett. **110**, 171801 (2013).
[8] P. A. R. Ade *et al.* (Planck Collaboration), Astron. Astrophys. **594**, A13 (2016).
[9] A. Gando *et al.* (KamLAND-Zen Collaboration), Phys. Rev. Lett. **110**, 062502 (2013).

[10] M. Agostini *et al.* (GERDA Collaboration), Phys. Rev. Lett. **111**, 122503 (2013).
[11] A. Gando *et al.* (KamLAND-Zen Collaboration), Phys. Rev. Lett. **117**, 082503 (2016).
[12] M. Agostini *et al.* (GERDA Collaboration), Nature (London) **544**, 47 (2017).
[13] K. Abe *et al.* (T2K Collaboration), Phys. Rev. D **91**, 072010 (2015).
[14] I. Esteban, M. C. Gonzalez-Garcia, M. Maltoni, I. Martinez-Soler, and T. Schwetz, J. High Energy Phys. 01 (2017) 087.
[15] K. Abe *et al.* (T2K Collaboration), Phys. Rev. Lett. **112**, 181801 (2014).
[16] P. Adamson *et al.* (MINOS Collaboration), Phys. Rev. Lett. **112**, 191801 (2014).
[17] A. Himmel (Super-Kamiokande Collaboration), AIP Conf. Proc. **1604**, 345 (2014).
[18] F. Capozzi, G. L. Fogli, E. Lisi, A. Marrone, D. Montanino, and A. Palazzo, Phys. Rev. D **89**, 093018 (2014).
[19] P. Vahle, talk given at the Neutrino 2016 Conference, 4–9 July 2016, London, United Kingdom, http://neutrino2016.iopconfs.org/home.
[20] R. Acciarri *et al.* (DUNE Collaboration), arXiv:1601.05471.
[21] R. Acciarri *et al.* (DUNE Collaboration), arXiv:1601.02984.
[22] T. Alion *et al.* (DUNE Collaboration), arXiv:1606.09550.
[23] C. Adams *et al.* (LBNE Collaboration), http://www.osti.gov/scitech/biblio/1128102, arXiv:1307.7335.
[24] D. Ayres *et al.* (NOνA Collaboration), arXiv:hep-ex/0503053.
[25] R. Patterson, talk given at the Neutrino 2012 Conference, 3–9 June 2012, Kyoto, Japan, http://neu2012.kek.jp/.
[26] S. K. Agarwalla, S. Prakash, and S. Uma Sankar, J. High Energy Phys. 03 (2014) 087.
[27] V. Barger, A. Bhattacharya, A. Chatterjee, R. Gandhi, D. Marfatia, and M. Masud, Phys. Rev. D **89**, 011302 (2014).
[28] N. Nath, M. Ghosh, and S. Goswami, Nucl. Phys. **B913**, 381 (2016).
[29] K. Bora, D. Dutta, and P. Ghoshal, Mod. Phys. Lett. A **30**, 1550066 (2015).
[30] K. Bora and D. Dutta, J. Phys. Conf. Ser. **481**, 012019 (2014).
[31] G. L. Fogli and E. Lisi, Phys. Rev. D **54**, 3667 (1996).
[32] K. Hiraide, H. Minakata, T. Nakaya, H. Nunokawa, H. Sugiyama, W. J. C. Teves, and R. Z. Funchal, Phys. Rev. D **73**, 093008 (2006).
[33] C. R. Das, J. Maalampi, J. Pulido, and S. Vihonen, arXiv:1606.02504.
[34] R. Gandhi, P. Ghoshal, S. Goswami, P. Mehta, and S. Uma Sankar, Phys. Rev. D **73**, 053001 (2006).
[35] T. Lee, Phys. Rev. D **8**, 1226 (1973).
[36] T. Lee, Phys. Rep. **9**, 143 (1974).
[37] V. Barger, A. Bhattacharya, A. Chatterjee, R. Gandhi, D. Marfatia, and M. Masud, Int. J. Mod. Phys. A **31**, 1650020 (2016).
[38] S. Prakash, S. K. Raut, and S. Uma Sankar, Phys. Rev. D **86**, 033012 (2012).
[39] S. Kumar Agarwalla, S. Prakash, and S. Uma Sankar, J. High Energy Phys. 03 (**2014**) 087.
[40] D. Dutta and K. Bora, Mod. Phys. Lett. A **30**, 1550017 (2015).
[41] K. Bora, G. Ghosh, and D. Dutta, Adv. High Energy Phys. **2016**, 9496758 (2016).
[42] P. O. Ludl and W. Grimus, J. High Energy Phys. 07 (2014) 090.
[43] M. Berger and K. Siyeon, Phys. Rev. D **64**, 053006 (2001).
[44] C. I. Low, Phys. Rev. D **70**, 073013 (2004).
[45] C. I. Low, Phys. Rev. D **71**, 073007 (2005).
[46] W. Grimus, A. S. Joshipura, L. Lavoura, and M. Tanimoto, Eur. Phys. J. C **36**, 227 (2004).
[47] Z.-z. Xing and S. Zhou, Phys. Lett. B **679**, 249 (2009).
[48] S. Dev, S. Gupta, and R. R. Gautam, Phys. Lett. B **701**, 605 (2011).
[49] T. Araki, J. Heeck, and J. Kubo, J. High Energy Phys. 07 (2012) 083.
[50] R. G. Felipe and H. Serodio, Nucl. Phys. **B886**, 75 (2014).
[51] A. Dighe and N. Sahu, arXiv:0812.0695.
[52] W. Grimus and L. Lavoura, J. Phys. G **31**, 693 (2005).
[53] Z.-z. Xing, Phys. Rev. D **69**, 013006 (2004).
[54] E. Lashin and N. Chamoun, Phys. Rev. D **85**, 113011 (2012).
[55] K. Deepthi, S. Gollu, and R. Mohanta, Eur. Phys. J. C **72**, 1888 (2012).
[56] R. R. Gautam, M. Singh, and M. Gupta, Phys. Rev. D **92**, 013006 (2015).
[57] L. M. Cebola, D. E. Costa, and R. G. Felipe, Phys. Rev. D **92**, 025005 (2015).
[58] P. H. Frampton, S. L. Glashow, and D. Marfatia, Phys. Lett. B **536**, 79 (2002).
[59] Z.-z. Xing, Phys. Lett. B **530**, 159 (2002).
[60] Z.-z. Xing, Phys. Lett. B **539**, 85 (2002).
[61] A. Kageyama, S. Kaneko, N. Shimoyana, and M. Tanimoto, Phys. Lett. B **538**, 96 (2002).
[62] S. Dev, S. Kumar, S. Verma, and S. Gupta, Phys. Rev. D **76**, 013002 (2007).
[63] P. Ludle, S. Morisi, and E. Peinado, Nucl. Phys. **B857**, 411 (2012).
[64] S. Kumar, Phys. Rev. D **84**, 077301 (2011).
[65] H. Fritzsch, Z.-z. Xing, and S. Zhou, J. High Energy Phys. 09 (2011) 083.
[66] D. Meloni and G. Blankenburg, Nucl. Phys. **B867**, 749 (2013).
[67] D. Meloni, A. Meroni, and E. Peinado, Phys. Rev. D **89**, 053009 (2014).
[68] S. Dev, R. R. Gautam, L. Singh, and M. Gupta, Phys. Rev. D **90**, 013021 (2014).
[69] S. Dev, L. Singh, and D. Raj, Eur. Phys. J. C **75**, 394 (2015).
[70] M. Borah, D. Borah, and M. K. Das, Phys. Rev. D **91**, 113008 (2015).
[71] S. Kaneko and M. Tanimoto, Phys. Lett. B **551**, 127 (2003).
[72] S. Kaneko, M. Katsumata, and M. Tanimoto, J. High Energy Phys. 07 (2003) 025.
[73] S. Dev and S. Verma, Mod. Phys. Lett. A **25**, 2837 (2010).
[74] M. Bando, S. Kaneko, M. Obara, and M. Tanimoto, Prog. Theor. Phys. **112**, 533 (2004).
[75] T. P. Nguyen, Mod. Phys. Lett. A **29**, 1450038 (2014).

[76] R. Kalita and D. Borah, Int. J. Mod. Phys. A **31**, 1650008 (2016).
[77] P. Huber, M. Lindner, and W. Winter, Comput. Phys. Commun. **167**, 195 (2005).
[78] P. Huber, J. Kopp, M. Lindner, M. Rolinec, and W. Winter, Comput. Phys. Commun. **177**, 432 (2007).
[79] Z.-z. Xing, arXiv:hep-ph/0406049.
[80] Jon Urheim, talk given at the Neutrino 2016 Conference, 4–9 July 2016, South Kensington, Landon, http://neutrino2016.iopconfs.org/programme.
[81] R. Acciarri *et al.* (DUNE Collaboration), arXiv:1601.05471.
[82] W. Rodejohann, Int. J. Mod. Phys. E **20**, 1833 (2011).
[83] K. Bora, D. Borah, and D. Dutta (to be published).